Choirs, HI Galaxy Groups:
Catalogue and Detection of Star-forming Dwarf Group Members

Sarah M. Sweet[1], Gerhardt Meurer[2,3], Michael J. Drinkwater[1], Virginia Kilborn[4], Helga Dénes[4], Kenji Bekki[2,3], Dan Hanish[5], Henry Ferguson[6], Patricia Knezek[7], Joss Bland-Hawthorn[8], Michael Dopita[9], Marianne T. Doyle-Pegg[1], Ed Elson[2,3], Ken Freeman[9], Tim Heckman[5], Robert Kennicutt[10,11], Ji Hoon Kim[12], Bärbel Koribalski[13], Martin Meyer[2,3], Mary Putman[14], Emma Ryan-Weber[10], Chris Smith[15], Lister Staveley-Smith[2,3], O. Ivy Wong[13], Rachel Webster[16], Jessica Werk[14], Martin Zwaan[17]

1: School of Mathematics and Physics, University of Queensland, Qld, 4072, Australia; sarah@sarahsweet.com.au;
2: School of Physics, University of Western Australia, 35 Stirling Highway, Crawley, WA, 6009, Australia;
3: International Centre for Radio Astronomy Research, ICRAR M468, 35 Stirling Highway, Crawley, WA, 6009, Australia;
4: Mail number H30, Swinburne University of Technology, PO Box 218, Hawthorn, Victoria 3122, Australia;
5: Infrared Processing and Analysis Center, California Institute of Technology, 100-22, Pasadena, CA 91125, USA;
6: Space Telescope Science Institute, 3700 San Martin Drive, Baltimore, MD, 21218, USA;
7: WIYN Consortium, Inc., 950N Cherry Avenue, Tucson, AZ, 85719, USA;
8: Sydney Institute for Astronomy, School of Physics, University of Sydney, Camperdown, NSW 2006, Australia;
9: Research School of Astronomy & Astrophysics, Mount Stromlo Observatory, Cotter Road, Weston Creek, ACT, 2611, Australia;
10: Institute of Astronomy, University of Cambridge, Madingley Road, Cambridge CB 0HA, UK;
11: Department of Astronomy, University of Arizona, 933 North Cherry Avenue, Tucson, AZ, 85721-0065, USA;
12: Center for the Exploration of the Origin of the Universe, Astronomy Program, Department of Physics and Astronomy,
Seoul National University, Seoul, Republic of Korea;
13: CSIRO Astronomy and Space Science, Australia Telescope National Facility, PO Box 76, Epping, NSW, 1710, Australia;
14: University of Michigan, 830 Dennison, 500 Church Street, Ann Arbor, MI, 48109-1042, USA;
15: Cerro Tololo Inter-American Observatory (CTIO), part of the National Optical Astronomy Observatory (NOAO),
Colina El Pino S/N, Casilla 603, La Serena, Chile;
16: School of Physics, University of Melbourne, Parkville, Victoria, 3010, Australia;
17: European Southern Observatory, Karl-Schwarzschild-Str. 2, D-85748 Garching b. München, Germany

1 May 2013

ABSTRACT

Hα observations centred on galaxies selected from the HI Parkes All Sky Survey (HIPASS, Barnes et al. 2001) typically show one and sometimes two star-forming galaxies within the $\sim$15' beam of the Parkes 64-m HI detections. In our Survey of Ionization in Neutral Gas Galaxies (SINGG, Meurer et al. 2006) we found fifteen cases of HIPASS sources containing four or more emission line galaxies (ELGs). We name these fields Choir groups. In the most extreme case we found a field with at least nine ELGs. In this paper we present a catalogue of Choir group members in the context of the wider SINGG sample.

The dwarf galaxies in the Choir groups would not be individually detectable in HIPASS at the observed distances if they were isolated, but are detected in SINGG narrow-band imaging due to their membership of groups with sufficiently large total HI mass. The ELGs in these groups are similar to the wider SINGG sample in terms of size, Hα equivalent width, and surface brightness.

Eight of these groups have two large spiral galaxies with several dwarf galaxies and may be thought of as morphological analogues of the Local Group. However, on average our groups are not significantly HI-deficient, suggesting that they are at an early stage of assembly, and more like the M81 group. The Choir groups are very compact at typically only 190 kpc in projected distance between the two brightest members. They are very similar to SINGG fields in terms of star formation efficiency (the ratio of star formation rate to HI mass; SFE), showing an increasing trend in SFE with stellar mass.

Key words: galaxies: dwarf – radio continuum: galaxies – galaxies: Local Group – galaxies: classification – galaxies: clusters: general – galaxies: clusters: individual

1   INTRODUCTION

Galaxies are arranged throughout the Universe in a hierarchy of environments ranging from clusters to groups, to isolation (e.g. Tully 1987; Kilborn et al. 2009; Pisano et al. 2011). Galaxies that reside within denser environments such as clusters are different to those at group densities and yet still different to those that lie in the field. The amount of star formation depends largely on the amount of gas available to fuel the process (Kennicutt 1989, 1998; Bergvall 2012). Moreover, at group densities, the ratio of star-forming spiral galaxies to less prolific elliptical galaxies is lower, so morphology is important as well (Wijesinghe et al. 2012). It is not known exactly how groups transition from gas and spiral-rich to gas-poor, elliptical-rich ones like those analysed by Kilborn et al. (2009); Mulchaey & Zabludoff (1998) so the picture is incomplete. Groups of galaxies are particularly interesting because the suppression of star formation begins at group densities (Lewis et al. 2002; Gómez et al. 2003).

The selection technique for star formation studies can lead to inherent biases in the sample. Previous authors have used Hα to select their samples (e.g. Gallego et al. 1995; Salzer et al. 2000). However, Hα followup imaging studies of optically selected galaxies are limited by the selection biases of their parent sample, typically excluding low surface brightness galaxies. The result is that these surveys are biased towards galaxies with high rates of star formation, and contain no control sample with low star formation rates.

In order to overcome that optical bias, we have selected galaxies based on their H I mass measured by the H I Parkes All-Sky Survey (HIPASS, Barnes et al. 2001; Koribalski et al. 2004; Meyer et al. 2004). With this sample we conducted the Survey for Ionisation of Neutral Gas Galaxies (SINGG), an Hα and R band imaging follow-up to HIPASS. Meurer et al. (2006) presents the SINGG sample, and gives data on 93 HIPASS targets observed for SINGG. Now a total of 292 HIPASS targets have been observed by SINGG with the CTIO 1.5m and 0.9m telescopes (Meurer et al. 2013, in prep). It is these images which form the basis of this study. Fifteen fields were discovered to contain four or more Hα sources and were dubbed Choir groups. The Choir member galaxies are different to typical field galaxies in that the larger galaxies are distorted and none are elliptical galaxies.

In this paper we present a catalogue of Choir group members. Section 2 outlines the sample selection and observations of SINGG. We present our catalogue of Choir group members in Section 3, along with a discussion of their properties in the context of SINGG. Section 4 concludes the paper.

We base distances on the Multipole model of Mould et al. (2000), with $H_0 = 70 \mathrm{kms}^{-1}\mathrm{Mpc}^{-1}$ as in Meurer et al. (2006). We adopt a Chabrier (2003) initial mass function (IMF).

2   SAMPLE SELECTION AND DATA

Our sample is drawn from the 292 HIPASS targets observed for SINGG. H I measurements are all from the HIPASS H I catalogue HICAT (Meyer et al. 2004), except for two groups (HIPASS J0443-05 and J1059-09). After noticing an anomalous H I mass for one group, we manually remeasured the H I mass of every Choir group. We found that the unusual H I profiles of the Choir fields caused the automated HIPASS parameterisation algorithm to fit poorly in these two cases. Our manually remeasured H I masses are used in this paper for these two fields.

The SINGG observations were mostly conducted at the Cerro Tololo Inter-American Observatory (CTIO) 1.5m telescope, whose field of view of 14'.7 matches the ∼ 15′ beam of the Parkes radiotelescope well. Additional observations were taken at the CTIO 0.9m telescope whose field of view is 13.5'.

Emission Line Galaxies (ELGs) in SINGG were identified by eye by two of us (DH, GRM) primarily using colour composites of the SINGG data where the red, green, and blue images of the display were assigned to the net Hα image, the narrowband image without any continuum subtraction, and the R band image respectively. The colour images are similar to those shown in Figure B1. ELGs are distinguished by having net line emission, and being noticeably more extended than a point source. For unresolved emission line sources (ELdots, Ryan-Weber et al. 2004; Werk et al. 2010) the distance is not clear. They may be detached H II regions revealed by Hα emission or background emitters of other lines (especially [O III] 5007) redshifted into our passband. Ancillary spectroscopy is needed to distinguish between these possibilities, and that is beyond the scope of this work; the ELdots in the Choir fields are not discussed further in this paper. The original data were consulted in cases where the reality of the line emission was not clear, i.e. low surface brightness or low equivalent width objects. The images were then measured using the standard SINGG data analysis pipeline (Meurer et al. 2006).

While most of the (H I-rich, 15'x15') fields in SINGG contain a single ELG, there are fifteen fields that have four or more ELGs. These fields of multiple SINGGers we name Choir groups, presented in Table 1.

Our working assumption is that the line emission results from Hα at a velocity similar to the HIPASS source, and hence that all ELGs in a field are physically associated. This is in the same manner as Tully et al. (2006), who argued that associations of dwarf galaxies in his sample were bound. For each field the narrow-band filter was chosen to most closely match the mean wavelength and wavelength range of the filter to the H I velocity profile of the field. The pivot wavelengths and transmission widths are listed in Table 1. Typically filters with bandwidth ∼ 30 Å were used for the narrow band images of these particular SINGG fields. This corresponds to ∼ 3000 km s⁻¹, much broader than the typical H I line widths involved. Therefore spectroscopic data are needed to firmly associate all ELGs with the HIPASS detection. We are in the process of confirming redshifts and these will be published in a future paper.

As this project progressed we noticed that some ELGs were missed in the original selection of the Choir fields. These included some small high surface brightness galaxies as well as low surface brightness and low equivalent width (EW) detections. We also found cases where the morphology of a single galaxy was better described as multiple merging or superposed galaxies. In those cases what distinguishes the companions as separate ELGs is a noticeable concentration in both Hα and the *R*-band continuum. HII regions, on the other hand are distinguished by having a relatively weak continuum above the local background and being unresolved or barely resolved in Hα.

After discovering a few instances of "new" ELGs, one of us (GRM) carefully examined all Choir fields, as well as SINGG fields with three ELGs. In total we found 13 new ELGs. These are distinguished in Table 2 by an asterisk (*). While we think the evidence is strong that all ELGs listed here are separate galaxies with real Hα emission, we caution that there are some borderline cases, such as HIPASS J1408-21:S6 where the line emission has a low surface brightness and is displaced from the parent galaxy. While we do believe our selection based on visual inspection is thorough, spatially varying biases and subjectivity are likely. For example, while a strong BCD candidate like HIPASS J1051-17:S6 may be recognized even if it is projected near a brighter companion, a small galaxy with only one or two modest HII regions, such as HIPASS J0205-55a:S9 is easily noticed when isolated, but may not be recognized as a separate galaxy if projected on or near a bright spiral. Hα concentrations along extended tidal arms, such as HIPASS J1250-20:S5,S6 are especially ambiguous. It is not clear whether they are separate tidal dwarf galaxies (e.g., Bournaud et al. 2007) or just transitional HII regions.

The new ELGs in the sample were not measured using the SINGG measurement pipeline, since it was not operational when the measurements were required. Instead basic mesaurements of position and fluxes were measured using IMEXAM in IRAF[1].

In summary, the following criteria must be met to satisfy our Choir group definition:

(i) HI detection in HIPASS;

(ii) four or more ELGs in a single field of view of ∼15';

(iii) where an ELG is defined by net Hα emission in an extended source.

We point out that the above is the *minimum* to define a Choir group. The definition has the following caveats:

(i) Choir groups can be larger than 15', with members outside of the field of view;

(ii) Choir groups can therefore belong to much larger structures, e.g. HIPASS J0400-52, which is in Abell 3193;

(iii) Choir groups require spectroscopic followup to confirm assumed physical association.

These caveats are discussed more fully in Section 3.

We present the Choir groups in Table 1, and key properties of the individual Choir group members in Table 2. These data are preliminary results on all the galaxies observed with the CTIO 1.5m and 0.9m telescopes for SINGG. Full results are in preparation and will be presented elsewhere (Meurer et al., in prep).

3 DISCUSSION

All the galaxies in SINGG have (by design) HI and all are detected in Hα, indicating that HI-rich, non-star-forming galaxies are rare (Meurer et al. 2006). Fields observed for SINGG usually contain single ELGs, with some doubles and triples, and more rarely four or more galaxies in a single pointing (our Choir groups). We use the entire SINGG dataset as our control sample against which we compare the Choirs galaxies. In this section, we discuss selection biases, analyse the Choir member galaxies in terms of size, equivalent width, luminosity and surface brightness, and then focus on the Choir groups' morphology, size, star formation rate and efficiency, and HI deficiency.

3.1 Selection biases

Although SINGG overcomes biases that are prevalent in optically-selected surveys, some selection effects are still present. The two major selection effects are 1. a selection of more massive sources, and 2. a bias towards more distant groups.

First, the SINGG sample is selected from HIPASS so that the nearest sources at each HI mass are preferentially chosen; combined with the HIPASS HI detection limit this means that distant, isolated, low-mass HI sources are not selected (see Figure 1). This is therefore also a selection effect for Choir groups. The detection limits are discussed in detail by Zwaan et al. (2004). At higher redshift (distance ≳30 Mpc) only the most massive HI sources are detected by HIPASS. These sources are so rare that we can not find many of these except by looking at these distances. Hence most of the high mass $M_{HI} > 10^{10} M_{\odot}$ sources selected for SINGG have $D > 30$ Mpc. SINGG can detect galaxies optically to fairly low stellar masses out to the full ∼150 Mpc distance limit of HIPASS. While the HI mass detection limit precludes us from detecting isolated dwarf galaxies at distances greater than about 30 Mpc, we can detect them at these distances when they are part of a more massive HI system. We illustrate this in Figure 1. Choir groups (blue stars), SINGG doubles and triples (grey triangles) and SINGG singles (light grey circles) all show increasing HI mass with distance.

In order to show the likely contribution of the individual galaxies within the Choirs to the system HI mass, we bring some basic correlations seen within SINGG to bear. Following Meurer et al. (2006) we define the gas cycling
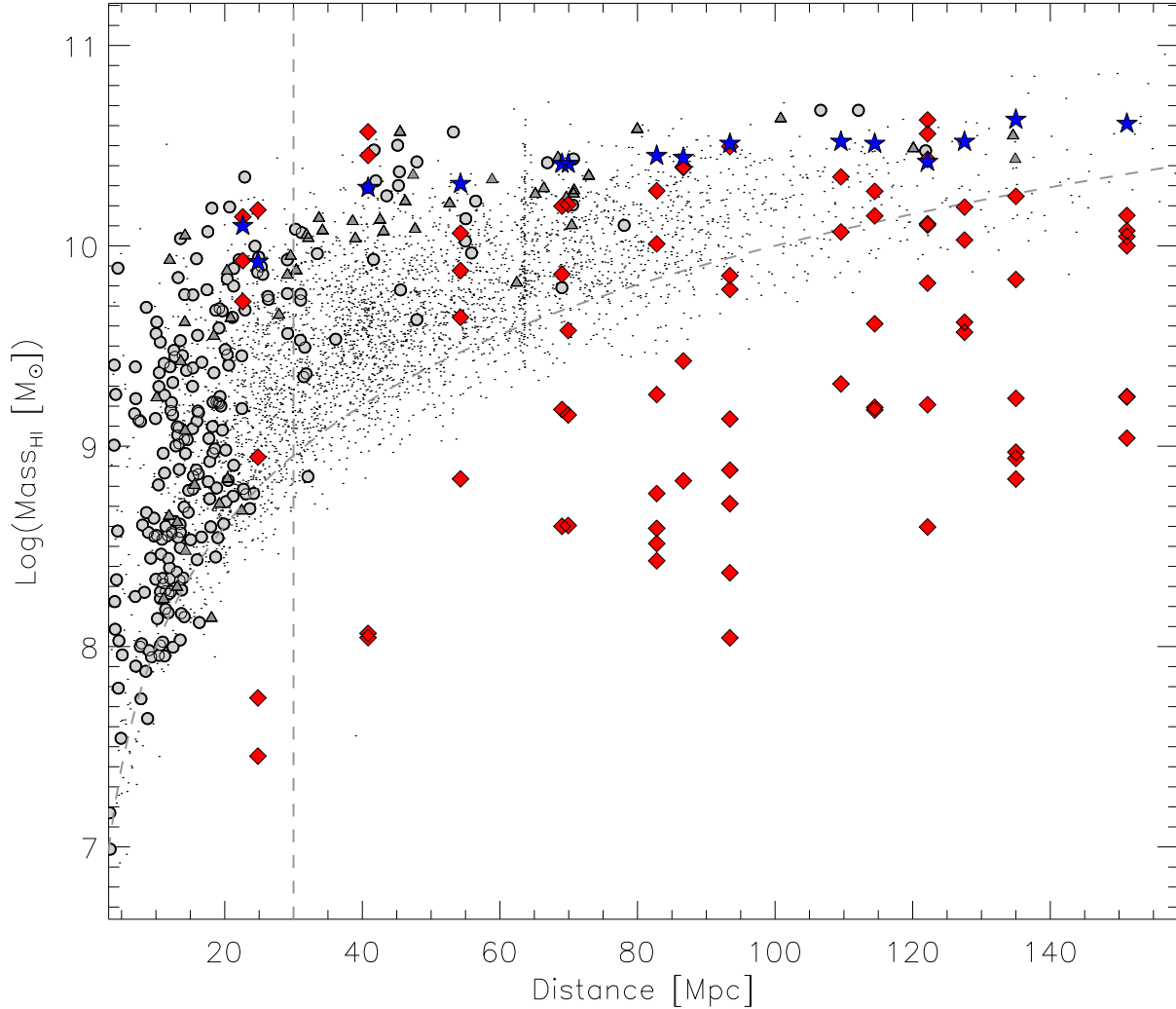
Figure 1. Total H<small>I</small> mass vs. distance for SINGG detections compared to H<small>I</small>PASS. The blue stars are Choir groups, mid grey triangles denote doubles and triples, and mid grey filled circles are single galaxies in SINGG. Black points indicate H<small>I</small>PASS detections not in SINGG. The vertical, dashed line at 30 Mpc represents the field of view limit for detecting an average Choir group. See text for explanation. The curved, dashed line represents the 3σ detection limit in H<small>I</small>PASS as described in Zwaan et al. (2004) and Meurer et al. (2006), from a fake source analysis and integrating over all line widths from 20 to 650 km s^{-1}. Choirs are at the high M_{HI} and large distance end of the distribution. Estimated H<small>I</small> mass for Choir member galaxies is shown as red diamonds. See text for calculation. Above the nominal group detection limit of 30 Mpc, only the brightest members of each group are detectable at the 3σ limit if isolated: the Choir dwarfs are only detected due to their inclusion in an H<small>I</small>-rich group.

time t_{gas}[yr] $= 2.3 M_{HI}/SFR$, where M_{HI} is the H<small>I</small> mass and the factor of 2.3 is a correction for molecular hydrogen and helium content. We then adopt the Meurer et al. (2009) conversion of star formation rate SFR [M$_\odot$ yr^{-1}] $= L_{H\alpha}/(1.5 \times 1.04 \times 10^{41})$, where $L_{H\alpha}$ is the $H\alpha$ luminosity in ergs/s. The factor of 1.5 converts the Salpeter (1955) IMF measurements of SINGG to a Chabrier (2003) profile (Brinchmann et al. 2004; Meurer et al. 2009). In Figure 2 we plot t_{gas} as a function of R-band effective surface brightness μ_e, with the best fit

$$\log(t_{gas}) = (4.14 \pm 0.48) + (0.29 \pm 0.02)\mu_e. \qquad (1)$$

This allows us to estimate M_{HI} from $L_{H\alpha}$ and μ_e as fol-

lows:

$$\log(M_{HI}) = \log(L_{H\alpha}) + (0.29 \pm 0.02)\mu_e - (37.42 \pm 0.48). \qquad (2)$$

The significance of this relation will be discussed in the context of SINGG in a future paper.

We use this relation to predict the H<small>I</small> mass of individual Choir member galaxies, shown as red diamonds in Figure 1. If the galaxies were isolated, only the brightest galaxies in each Choir group could be detected in H<small>I</small> by Parkes. The smaller members of the Choir groups could not be detected, and are only included in SINGG due to their inclusion in an H<small>I</small>-rich group. The groups at 40 and 120Mpc, H<small>I</small>PASS J1403-06 and J1059-09, each have a total *observed* H<small>I</small> mass
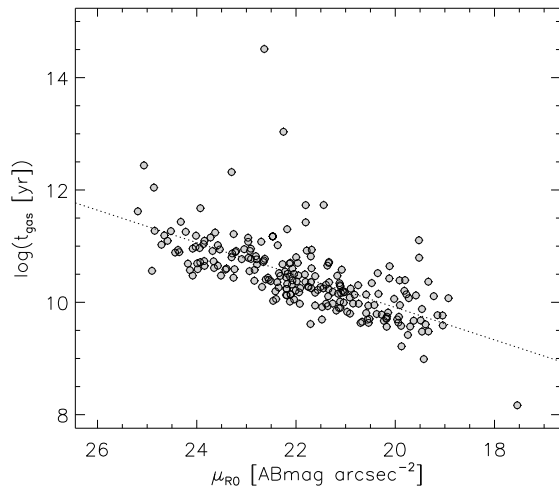
Figure 2. Parameterisation of gas cycling time as a function of *R*-band effective surface brightness for single galaxies in SINGG.

Figure 3. HI mass histogram and distance histogram of SINGG detections. Blue colours correspond to Choir groups; darker colours correspond to more members (see key). These histograms are nested, so that the entire area covers the whole SINGG sample. Choirs are at the high M_{HI} and large distance end of the distribution.

less than the *predicted* HI mass of their two-three brightest members. This means that these groups are both deficient in HI compared with the amount expected based on the Hα luminosity and $R-$band surface brightness of their group members. See Section 3.7 for a discussion of HI deficiency.

The second selection effect is a bias towards more distant groups; there are fewer Choir groups and fewer members per group detected at small distances. This is because the large angular size of nearby groups is more likely to exceed our 15' field of view. A single pointing will then contain fewer than all of the members in a group, leading to underrepresentation of the number of galaxies identified as group members. (We note previously detected giants that are likely to be asssociated with our Choir groups in Appendix A.) Also, if a pointing contains less than four objects (the threshold for defining a Choir), a group will not be detected, leading to underrepresentation of number of groups at small distances.

For a Choir group to be detected, it must have at least four ELGs within the field of view. We characterise group size by measuring the projected distance between the two most luminous galaxies in each group. (See Section 3.5.) Our mean Choir group size is 190 kpc, which will fit inside a single pointing as near as $\sim$ 30 Mpc. Therefore, we do not expect to see any groups of this average size nearer than 30 Mpc (represented by the vertical dashed line in Figure 1). This corresponds closely with our observations; although there are two groups below this cut, one is very compact (HIPASS J1159-19) and the other barely makes the Choir definition with one member nearly outside of our field of view (HIPASS J2318-42a).

It is important to note that many of the nearby SINGG galaxies are likely to be in groups where only three or fewer galaxies fit within the SINGG field of view. We estimate the fraction of SINGG that is in groups similar to the Choirs by measuring the proportion of Choir groups compared with
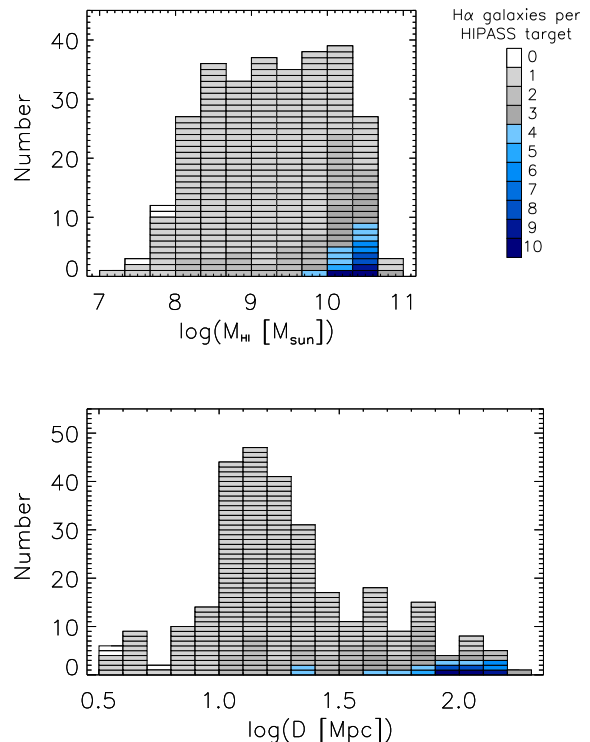
all SINGG detections at distances greater than 30 Mpc. In this manner we calculate that 20% of SINGG detections are in fact in galaxy groups. Considering that Choir groups are still likely to be under-represented at the near end of this distance range, the true fraction may be significantly higher. The proportion of groups increases with distance. According to Tully (1987), around 50% of galaxies are expected to be in groups of 4 or more members.

These two selection effects mean that Choirs are among the most distant and HI-massive of the HIPASS sources. Figure 3 illustrates the distribution of groups in both HI mass and distance. While the SINGG control sample has (by design) a relatively flat distribution between $8 < log(M_{HI}) < 10.6$, the number of Choir groups peaks at the high-mass end of this range. These differences must be taken into account when comparing Choirs with the control SINGG sample for distance-dependent and mass-dependent quantities.

In the following subsections we continue this discussion with an analysis of the properties of the Choir member galaxies.

3.2 Size and Equivalent Width

The histogram of *R*-band effective (half-light) radius, $r_e(R)$ for Choir member galaxies, in comparison to other sin-
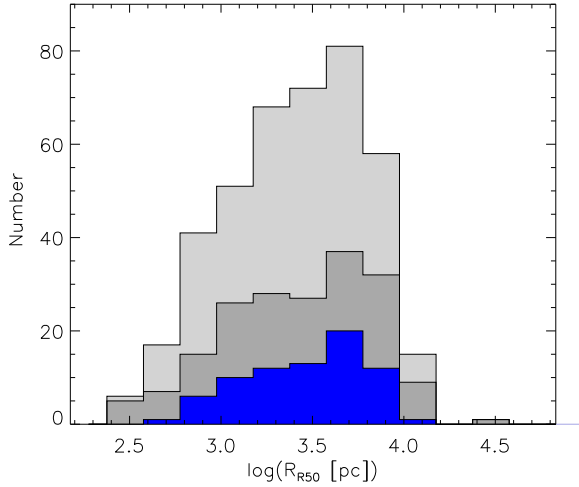
Figure 4. Histogram of R-band half-light radius of ELGs in SINGG. Blue, mid grey and light grey denote Choir member galaxies, SINGG doubles and triples, SINGG single galaxies respectively. Choir members are not significantly different from the control SINGG sample ($p = 0.35$). This is similar for Hα half-light radius, R-band radius enclosing 90% of flux, Hα radius enclosing 90% of flux. The same is seen when R > -21 to compare only dwarf galaxies.

Figure 5. Hα EW calculated within the effective radius and corrected for dust. Blue, mid grey and light grey denote Choir member galaxies, SINGG doubles and triples, SINGG single galaxies respectively. Choir members do not have high EW for their size ($p = 0.54$). The same is seen when R > -21 to compare only dwarf galaxies.

gle and multiple SINGG galaxies, is shown in Figure 4. A Kolmogorov-Smirnov (KS) test shows that Choir members are not significantly different from the single detections in SINGG with a fractional probability that they were drawn from the same parent sample of $p = 0.35$. A similar result occurs for Hα effective radius, radius enclosing 90% of R-band flux and radius enclosing 90% of Hα flux. Figures demonstrating this are not shown for the sake of brevity. Applying a magnitude cut at $M_R > -21$ to exclude the most luminous galaxies does not alter the result; lower luminosity Choir galaxies are also not significantly different from their SINGG counterparts.

Figure 5 is a histogram of Hα equivalent width (measured within the Hα effective radius and corrected for dust absorption). Choir members do not have high EWs when compared with the SINGG control sample ($p = 0.54$). The same result is seen for lower luminosity galaxies ($M_R > -21$).

Naively, one might expect the distance-dependent detection limit in H I mass, together with the fact that Choirs are at further distances, to cause a dependence of radius and EW on distance as well. However, as discussed above, Choir dwarfs are included in the SINGG field of view only because of their proximity to H I-detectable giants. We have used the Choir groups to identify star-forming dwarfs at such large distances that they are not detectable in H IPASS, but their optical properties are the same as nearby star-forming dwarfs detected in H IPASS.

3.3 Luminosity and Surface brightness

In Figures 6 and 7 we plot luminosity-surface brightness and luminosity-radius correlations. Choir galaxies have on aver-
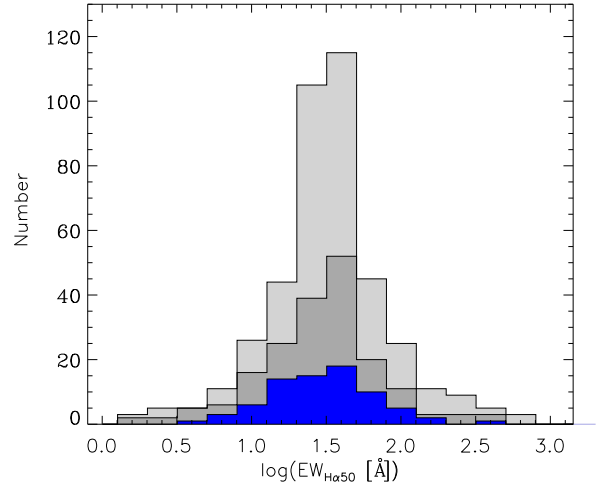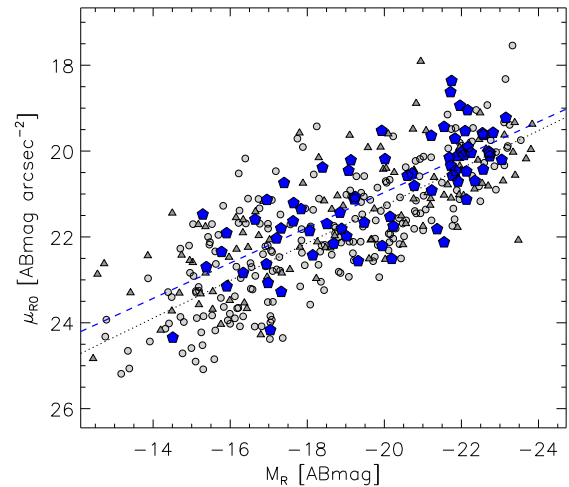

Figure 6. Surface brightness in R-band as a function of absolute magnitude. The blue pentagons are Choir member galaxies, mid grey triangles denote doubles and triples, and mid grey filled circles are single galaxies in SINGG. The blue, dashed line is a linear fit to Choir members and the dotted line is for single galaxies in SINGG. The small offset is not significant ($p = 0.06$).

age 0.5 dex higher surface brightness and 0.05 dex smaller radius for their luminosities than the control sample. We perform a KS test on the distribution of $\{y - (a + bx)\}$, where y is the surface brightness or radius and x is the R-band magnitude of the Choir galaxies, and a and b are parameters from the fit to single galaxies in SINGG. We find that the offsets are not significant, with p-values of 0.06 and 0.27 respectively.
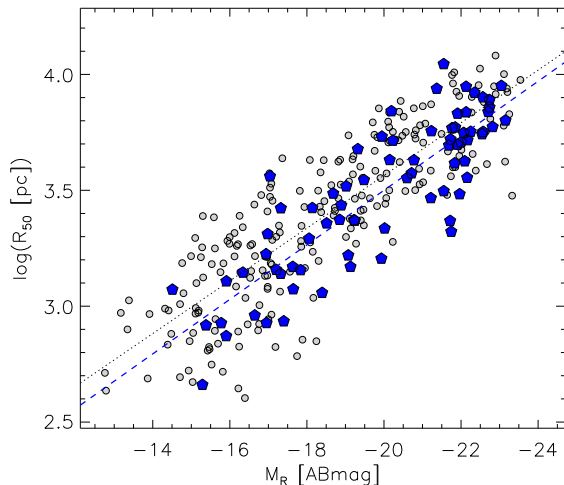
Figure 7. *R*-band half-light radius as a function of absolute magnitude. The blue pentagons are Choir member galaxies, mid grey triangles denote doubles and triples, and mid grey filled circles are single galaxies in SINGG. The blue, dashed line is a linear fit to Choir members and the dotted line is for single galaxies in SINGG. The small offset is not significant ($p = 0.27$).

3.4 Group morphology

The Choir groups by definition have four or more Hα-emitting galaxies, without further restriction on morphology or relative size. An interesting subset (eight out of fifteen groups) is groups that are comprised of two large spirals and two to eight smaller galaxies. We illustrate this in Figure 8 where we show *R*-band absolute magnitude of Choir members relative to the brightest member in each group. The peak at -0.25 mag represents the second-largest giant, and the extended tail peaking at -2.25 mag represents dwarf companions. We note that M_r magnitudes for the Milky Way (MW), M31, Large Magellanic Cloud (LMC) and Small Magellanic Cloud (SMC) are -21.17, -21.47, -18.60 and -17.20 respectively (Robotham et al. 2012), so that the Local Group will appear on this plot at the white arrows. In terms of luminosity the Choir groups therefore appear to be possible Local Group (LG) analogues, as discussed by Pisano et al. (2011); Robotham et al. (2012). Our selection method seems to be good at finding LG analogues (at least in terms of *magnitude* and *morphology*), with an approximate strike rate of 50%. We suggest that perhaps these types of groups are more common than previously thought, but usually the dwarf galaxies fall below the relevant detection limit so the group appears as a pair of bright spirals. In SINGG however, star-forming dwarf galaxies are readily apparent in the Hα imaging.

In Appendix A we point out some morphological features of each Choir group and search larger photographic survey images to check for possible group members outside of our imaging. Interestingly, there are no *bright* ellipticals in the SINGG imaging, and the few nearby giant ellipticals do not appear to be associated with the HIPASS detections. This is in contrast with optically- and X-ray-selected groups where the elliptical fraction is 0.4 to 0.5 (Mulchaey 2000). The
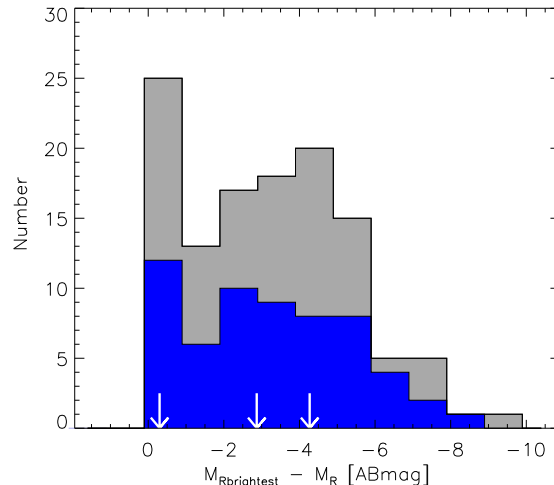

Figure 8. Distribution of relative luminosities of group galaxies compared to the most luminous in each group. The blue area denotes Choir member galaxies, mid grey denotes doubles and triples in SINGG. Single galaxies in SINGG are not shown, as there are no fainter companions in these fields. The first peak indicates when there are two large galaxies in a group and the second broader peak shows the dwarf members. The white arrows denote the position of Local Group members relative to M31 (left to right: MW, LMC, SMC). Qualitatively, our groups have a similar distribution of relative *R*-band magnitude to our Local Group.

discrepancy is probably a consequence of the HI selection in HIPASS being biased towards younger, HI-rich groups with fewer ellipticals.

3.5 Group compactness

In this section we compare the size of our Choir groups to Hickson Compact Groups (HCGs, Hickson et al. 1989) and groups in the Garcia (1993) catalogue. These three catalogues all contain groups of four or more members, but have different limiting magnitudes and distance ranges, and different group-finding algorithms.

Ideally, galaxy group size is measured by the virial radius defined as the radius enclosing a luminosity brighter than a specified magnitude (e.g., Tully 1987; Garcia 1993, 1995). This measurement requires radial velocity data, which do not yet exist for most of our Choir group members. It also assumes a relaxed group with a Gaussian distribution of velocities, but our Choir groups are not relaxed and do not have a sufficient number of members to display a Gaussian distribution. We are limited by having only a few members, particularly in the majority of cases where there are only two bright spirals and a number of faint dwarfs. While it may appear possible to use the projected distance between two closest neighbours in the group to compare our groups to other samples, this statistic should only be used to compare catalogues that have consistent limiting magnitudes, which is not the case for Choirs, HCGs and Garcia groups. We therefore use the projected distance between the two *most luminous* galaxies in each group as a measurement of

'group compactness'. This parameter is not as physical as previously-mentioned measurements of group size, but simply allows us to put our groups in context with existing catalogues given the available data. We emphasise that our comparison is not strict, because the catalogues are based on different algorithms.

For each of the three catalogues we calculate the compactness parameter and show histograms for the different catalogues in Figure 9. Mean group compactnesses for Choir groups, Hickson groups and Garcia groups are 190 ± 31, 87 ± 8 and 961 ± 52 kpc respectively. The distributions are significantly different; a KS test yields $p < 0.001$ that Choir groups and Garcia groups belong to the same population, and $p < 0.001$ that Choir groups and Hickson groups belong to the same population. Of course, Choir group sizes are limited by the field of view of the CTIO images, causing our distribution to be skewed in favour of smaller groups; at our mean distance of 87 Mpc the maximum size of our groups is only 380 kpc.

For the Local Group this group compactness statistic is 800 kpc in 3D space. Using the typical $\sqrt{2}$ conversion factor, this corresponds to 565 kpc in 2D space. This is just over 3σ larger than our mean Choir group compactness. In terms of physical separation then, we note that Choirs appear to be a compressed version of the Local Group, and may represent a later stage of evolution of a system like M31 and the MW with their retinue of dwarfs.

A more sophisticated analysis that includes radial velocity measurements for a stricter definition has recently been conducted for the Galaxy And Mass Assembly sample (GAMA, Robotham et al. 2012), with the result that LG analogues are rare in that sample. We plan to conduct a similar analysis of the frequency of LG analogues in SINGG.

3.6 Star formation

In Figures 10 and 11 we plot specific star formation rate (sSFR) and total (group) star formation efficiency (SFE_T) as a function of stellar mass M_*, where $sSFR = SFR/M_*$ and $SFE_T = SFR_T/M_{HI,T}$. The subscript $_T$ denotes total quantities for each group. Stellar masses are estimated using the Bell et al. (2003) conversion $\log(M_*/L_g) = -2.61 + 0.298\log(M_*h^2/M_\odot)$, with $M_{R\odot} = 4.61$, $M_{g\odot} = 5.45$ and $(g-r) = 0.5$ mag for late-type galaxies (Blanton et al. 2003). This gives $\log(M_*) = -3.66 + 1.425\log L_R$. We note that West et al. (2009) found the Bell et al. (2003) conversion to be biased by emission lines within the SDSS broadband filters, particularly for the bluest galaxies. However, the EWs in our sample are low (Fig 5) compared with the ~ 1000 Å R-band filter, so the corrections are small and the conversion is adequate for our purposes.

In terms of both sSFR and group SFE_T, Choir galaxies fall neatly on the best fits to the control SINGG sample, with a KS p-value of 0.37 and 0.14 respectively[2]. This seems in con-

---

[2] In this section we perform the KS test on the distribution of $\{y - (a + bx)\}$, where y is the sSFR or SFE, x is the stellar mass of the Choir (SINGG) galaxies, and a and b are parameters from
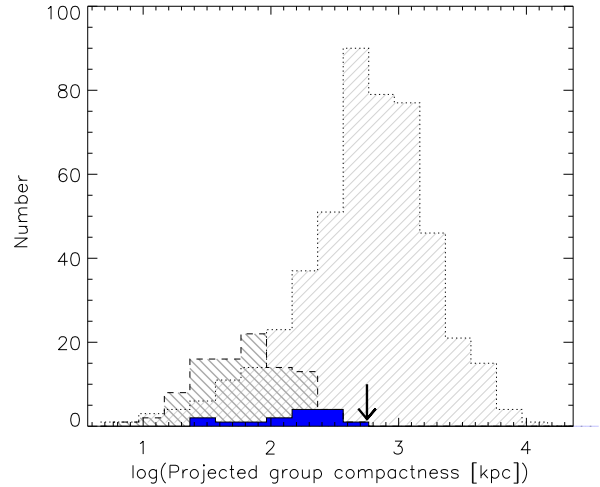

Figure 9. Choir group compactness, estimated by measuring separation between two brightest galaxies in a group. The solid, blue histogram is our Choir groups; light grey SW-NE cross-hatching with dotted outline is Garcia groups; medium grey NW-SE cross-hatching with dashed outline is Hickson groups. Our groups are more compact than Garcia groups, but not as compact as Hickson groups. The black arrow indicates the compactness of our Local Group, which is more than 3σ from the mean Choir group compactness.

trast to previous findings that star formation is suppressed at group densities (Lewis et al. 2002; Gómez et al. 2003). However, our selection is different in that typical group catalogues have at least four similarly large galaxies, and are insensitive to the dwarf members. Moreover, our control sample does not consist solely of isolated galaxies; as discussed earlier, at least 20% of the sample detections are likely to be in similarly dense groups of four or more member galaxies.

We therefore compare the star formation activity for our control sample to the work by Schiminovich et al. (GALEX Arecibo SDSS survey, GASS, 2010) and Huang et al. (Arecibo Legacy Fast ALFA (ALFALFA) survey with SDSS and GALEX photometry, 2012).

Firstly, our control sample exhibits a lower sSFR (by ~ 1 dex across the corresponding stellar mass range) than the high-sSFR trend of Schiminovich et al. (2010), with a KS test p-value < 0.001. This agrees with our suggestion that many of the galaxies in SINGG are not field galaxies but instead exist in Choir-like groups. Our SINGG sample is more consistent with the ($M_* > 9.5$) sSFR trend in Huang et al. (2012), although their sample shows a much steeper slope than ours. The SINGG data also hint at a transition to lower sSFR above a turnover stellar mass as seen in Bothwell et al. (2009) , but not convincingly so.

Next, our SFE_T plot (Figure 11) is for *groups*, not indi-

---

the fit to single galaxies in SINGG (galaxies in Schiminovich et al. (2010)). For the SINGG-Schiminovich comparison we perform the KS test on the subset of stellar masses within the domain of the Schiminovich et al. (2010) sample.

vidual galaxies, but according to Rownd & Young (1999) there should be no variation in SFE with environment. On this basis we compare our SFE data in Figure 11 to Schiminovich et al. (2010) and Huang et al. (2012). Our SFE for all of SINGG is lower than the high-sSFR (log $SFR/M_{star} > -11.5$) Schiminovich et al. (2010) data within the corresponding stellar mass range, with a KS-test p-value < 0.001. Our sample shows increasing SFE with stellar mass, in contrast with the Schiminovich et al. (2010) data, which do not seem to show any trend. We note that SINGG covers a much wider stellar mass range than the Schiminovich et al. (2010) sample, which may make the small trend more apparent in our work. Our results are more consistent with Bothwell et al. (2009) who found that gas cycling time ($\propto SFE^{-1}$) decreases shallowly with luminosity (that is, SFE increases slowly with luminosity) for HI-selected galaxies. Similarly, the SFE work by Huang et al. (2012) also is consistent with our SINGG sample.

We consider the source of discrepancy between our results and those of Schiminovich et al. (2010) and Huang et al. (2012). Neither we nor Schiminovich et al. (2010) correct for helium content when calculating sSFR or SFE but both correct for dust absorption. Both assume a Chabrier (2003) IMF. We point out that our SFRs are calculated from Hα emission, while the Schiminovich et al. (2010) SFRs are calculated from UV measurements. These indicators for star formation are sensitive to different types of stars; Hα probes the formation of the most massive stars ($M_\star > 20M_\odot$) which have lifetimes < 7 Myr, while UV traces the formation of stars down to $\sim 3M_\odot$ which have lifetimes up to 300 Myr (Meurer et al. 2009). We converted the NUV-based SFR calibration used by Schiminovich et al. (2010) into the Hα-based calibration of Meurer et al. (2009) and found that our calibration should yield SFRs 0.2 dex lower than Schiminovich et al. (2010) - that is, in the opposite direction to the displayed discrepancy.

While our sample is selected by HI mass, the Schiminovich et al. (2010) sample has a UV flux-limited selection, biasing their sample towards higher UV-SFRs. The higher redshift range (z<0.05) and consequent larger volume of their sample also allows a higher average HI mass and SFR. Similarly, the Huang et al. (2012) sample is also a flux-limited, HI-selected sample with a higher redshift than SINGG. The brighter and highest-redshift bins have a steep sSFR slope due to the flux limit, while nearby, volume-limited bins have a shallower slope. The combination of these two extremes results in the apparent turnover in their relation (Drinkwater et al., in prep). The difference between our sample and Huang et al. (2012) also includes different algorithms for calculating $M_\star$ and SFR to those we use. They use spectral energy density (SED) fitting to get both these quantities, and note that the $M_\star$ estimates are primarily dependent on the reddest fluxes while the SFR estimates come primarily from UV fluxes. We conclude that the differences between our results and those of Huang et al. (2012) and Schiminovich et al. (2010) are due to differences in sample selection and the calibration of the quantities involved.
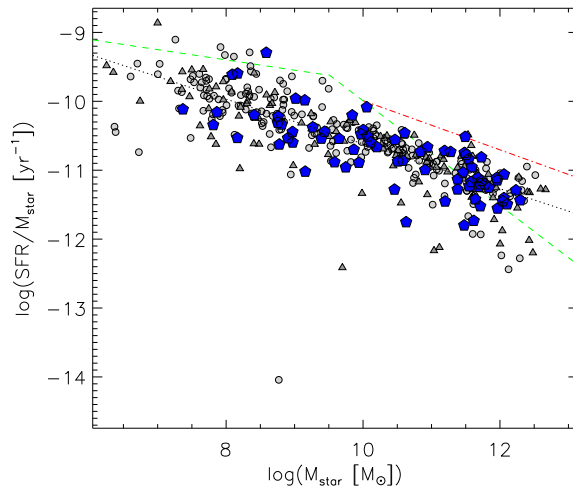

Figure 10. Specific star formation rate as a function of stellar mass for individual galaxies in SINGG. The blue pentagons are Choir member galaxies, mid grey triangles denote doubles and triples, and mid grey filled circles are single galaxies in SINGG. The black, dotted line is the best fit to single galaxies in SINGG. The red, dot-dashed line is the best fit to high-sSFR galaxies in Schiminovich et al. (2010). The green, dashed line is the Huang et al. (2012) relation. Choir galaxies lie on the relation defined by the control SINGG sample ($p = 0.37$). The SINGG sample exhibits a lower specific star formation rate than the Schiminovich sample across all stellar masses ($p < 0.001$). The high stellar mass Huang relation is better matched to the SINGG sample but displays a much steeper slope.
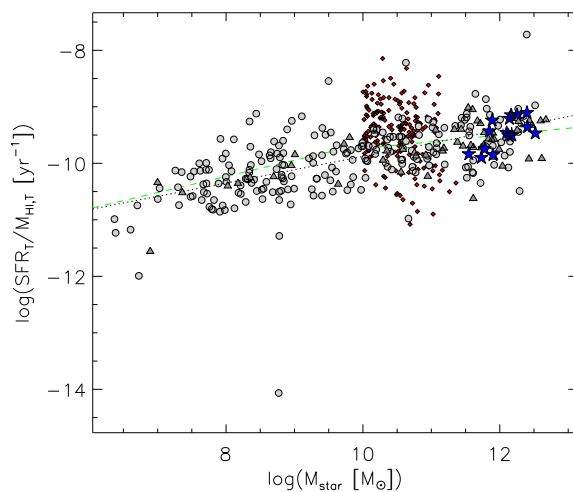

Figure 11. Total star formation efficiency as a function of total stellar mass for groups in SINGG. The blue stars are Choir groups, mid grey triangles denote doubles and triples, and mid grey filled circles are single galaxies in SINGG. The black, dotted line is for single galaxies in SINGG. The small, red diamonds are the high-sSFR galaxies in Schiminovich et al. (2010). The green, dashed line is the ridge line of the Huang et al. (2012) sample. Choir groups lie on the relation defined by the control SINGG sample ($p = 0.14$). The SINGG sample has a lower star formation efficiency than the high-sSFR Schiminovich sample within the corresponding stellar mass range ($p < 0.001$).

3.7 H I **Deficiency**

In general, galaxies in high density environments such as galaxy clusters and groups have less H I than galaxies of the same size and luminosity residing in the field (Haynes & Giovanelli 1983; Solanes et al. 2001; Kilborn et al. 2009). This deficiency in H I is quantified by the H I deficiency parameter, defined as the difference between the logarithms of the expected (M_{HIexp}) and observed H I mass (M_{HIobs}) of a galaxy (Haynes & Giovanelli 1983):

$$\text{DEF}_{HI} = \log[M_{HIexp}] - \log[M_{HIobs}].$$

An H I deficiency parameter of 0.3 dex translates into half the H I mass that we would expect a galaxy to have based on its optical luminosity or size. We consider an H I deficiency between -0.3 and 0.3 as normal H I content, as per Kilborn et al. (2009). In this section we exclude HIPASS J0205-55 due to the two HIPASS detections (see Appendix A), and HIPASS J2318-42a because one member is not completely within our field of view.

We used two independent methods to calculate the expected H I content for the Choir group galaxies. Our first method is to use the H I scaling relation in Dénes et al. (2013, in prep.). This relation is found from an analysis of the HOPCAT (HIPASS optical catalogue, Doyle et al. 2005) and gives H I mass (M_{HI}) as a function of SuperCosmos R-band magnitude ($Mag_{R_{SC}}$):

$$\log(M_{HI}) = 3.82 - 0.3 Mag_{R_{SC}}$$

We compared the SuperCosmos R-band magnitudes in HOPCAT to our SINGG R-band (AB) magnitudes ($Mag_{R_{AB}}$) and found them to scale by $Mag_{R_{SC}} = 8.7 + 1.36 Mag_{R_{AB}}$.

The inherent scatter in this relation is ± 0.3 dex. We then summed over all the members in each group and compared this to the measured H I content to calculate the total H I deficiency for each group. Our results are presented in Figure 12 (upper panel).

Our second method for calculating the expected H I content is to use Equation 2 from this paper, which gives H I mass based on Hα luminosity and R-band surface brightness. This is shown in the lower panel of Figure 12. Again, nearly all of our groups have normal H I content, with the exception of HIPASS J1059-09 and J1403-06, the two groups with the highest Hα luminosity in our sample. The members of these two groups also have a high surface brightness, resulting in the highest total predicted H I mass in our sample. In fact, the two to three brightest members in both groups all have a higher predicted H I mass than the corresponding groups themselves (see Fig 1). The uncertainty in the H I mass measurements of $\sim$ 10% (Koribalski et al. 2004), or 0.04 dex is negligible compared with the inherent scatter in Equation 2 of 0.48, so we adopt 0.48 dex as the uncertainty in H I deficiency. Hence the deficiency of these two groups is not statistically significant in our definition.

The two different methods produce slightly different results because the scaling is based on different physical properties. That is, method (1) identifies groups as H I deficient when their stellar luminosity is high compared to their H I mass, while deficient groups in method (2) have a high SFR for their H I mass. The implication is that the two groups that are deficient by method (2) and not (1) are dominated by high Hα equivalent width starbursting galaxies.

The fact that the Choir groups show no significant H I deficiency is a similar result to Kilborn et al. (2009) who showed an average lack of H I deficiency for their sample of optically-selected loose galaxy groups. The situation is less clear for compact groups, with Stevens et al. (2004) finding no significant H I deficiency, while Borthakur et al. (2010), found the typical H I deficiency of their sample of Hickson compact groups to be between 0.2-0.4 dex; in several cases the deficiency exceeded 0.5 dex.

We also compare the Choir groups to the gas-rich M81 group, as modelled by Nichols & Bland-Hawthorn (2011) in order to explain the H I deficiency of the LG (Grcevich & Putman 2009). They found that the M81 group must have commenced assembly at $z \sim 2$, in contrast to the LG which must have started by $z \sim 10$. The overall lack of H I deficiency of the Choir groups suggests that the group environment has not yet removed substantial amounts of H I gas from these groups. Hence the Choir groups are at an early stage of assembly. In the local context, this would make them more like the M81 group than the LG. Consequently we expect that, like the M81 group, the Choir groups have a larger system of HI clouds than the LG does. The fact that the Choir groups are gas-rich and less evolved than the Local Group indicates that they may provide important information about how gas enters groups and galaxies.

4 CONCLUSIONS

In this paper we have presented the Choirs: fields of four or more Hα-emitting galaxies found in the Survey for Ionisation for Neutral Gas Galaxies (SINGG). We found fifteen such groups in SINGG.

We make the following points:

(i) Due to selection effects, Choirs groups are at the large distance, high mass end of the parent SINGG sample of H I sources.

(ii) Choir member galaxies are not significantly different from the control SINGG sample in any of our measures of radius, Hα equivalent width, R-band surface brightness, specific star formation rate or star formation efficiency.

(iii) The dwarf galaxies in our Choir groups are not detectable on their own in HIPASS, but are detected in SINGG because the entire group has sufficient H I to be selected in HIPASS.

(iv) Within the limitations of the SINGG imaging field of view, there are no giant elliptical galaxies in the Choir groups.

(v) Eight of the fifteen Choir groups are characterised by having two giant spiral galaxies and a number of smaller galaxies. In terms of *morphology* they can be considered to be Local Group analogues.
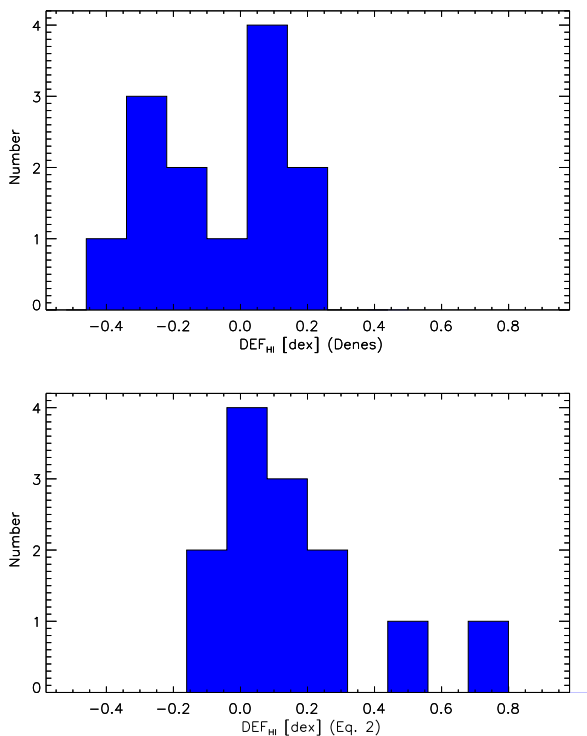
Figure 12. Distribution of H<small>I</small> deficiency parameter DEF_{HI} for each Choir group, defined as the logarithmic difference between observed group H<small>I</small> mass and predicted group H<small>I</small> mass (determined by summing the predicted H<small>I</small> masses of the individual group galaxies). Our groups are on average not significantly H<small>I</small> deficient. Upper panel: expected H<small>I</small> mass based on R-band magnitude. Lower panel: expected H<small>I</small> masses based on our Equation 2. Two very Hα-luminous groups, HIPASS J1059-09 and J1403-06 are not significantly H<small>I</small> deficient in this definition.

(vi) The mean group projected size is very compact at 190 kpc; much smaller than groups in the Garcia (1993) catalogue at 961 kpc, although not as compact as Hickson et al. (1989) Compact Groups at 87 kpc. The mean Choir compactness is also more than 3σ smaller than the same statistic for the Local Group. We note that our group size is limited by the field of view, with a maximum size of 380 kpc at the mean distance of 87 Mpc.

(vii) The specific star formation rate (sSFR = SFR/$M_\star$) of Choir member galaxies falls on the same $M_\star$ scaling relation as the rest of SINGG. This scaling relation is similar to what is found by for the ALFALFA HI selected survey (Huang et al. 2012). However, galaxies from the $M_\star$-selected GASS survey (Schiminovich et al. 2010) have sSFR 0.5 dex higher than our sample. Differences in the selection of the different samples, the depth of the observations, and the SFR calibrations are likely to account for the differences between these surveys.

(viii) The star formation efficiency (SFE = SFR/M_{HI}) of the Choir groups matches the sample of remaining SINGG members, which in turn is lower than the portion of the Schiminovich et al. (2010) sample with high sSFR. Our SINGG sample shows an increasing trend in SFE with stel-

lar mass, consistent with Bothwell et al. (2009) and Huang et al. (2012).

(ix) On average our groups are not significantly H<small>I</small> deficient, unlike typical groups of galaxies. This suggests an earlier stage of assembly than the Local Group, and more like the M81 group (Nichols & Bland-Hawthorn 2011).

(x) Our results indicate that emission line selection is an efficient way to pick out candidate galaxy groups in blind H<small>I</small> surveys. This can be very important when the beam size is large compared to the separations of galaxies within groups. Here, it is the Hα imaging that allows the small ELGs to be identified as likely dwarf group members. In comparison, astronomers using UV imaging alone to identify ELGs (e.g. Huang et al. 2012) may be reluctant to identify the smaller sources as dwarf members without follow-up spectroscopy.

In summary, H<small>I</small> combined with Hα selection can result in the selection of H<small>I</small>-rich groups. These are fairly compact and typically contain sources with strong signs of interaction, although global properties appear fairly normal. In approximately half of the cases, the groups are similar to the Local Group in containing two bright large spirals and numerous dwarf galaxies, although the compactness suggests the groups are at a more advanced stage of interaction than the LG. The lack of H<small>I</small> deficiency suggests that the groups are at an earlier stage of group assembly, more like the M81 group.

REFERENCES

Barnes, D. G. et al. 2001, MNRAS, 322, 486

Bell, E. F., McIntosh, D. H., Katz, N., & Weinberg, M. D. 2003, ApJS, 149, 289

Bergvall, N. 2012, Star Forming Dwarf Galaxies (Springer-Verlag, Berlin), 175

Blanton, M. R. et al. 2003, ApJ, 592, 819

Borthakur, S., Yun, M. S., & Verdes-Montenegro, L. 2010, ApJ, 710, 385, 0912.0297

Bothwell, M. S., Kennicutt Jr, R. C., & Lee, J. C. 2009, MNRAS, 400, 154

Bournaud, F. et al. 2007, Sci, 316, 1166, 0705.1356

Brinchmann, J., Charlot, S., White, S. D. M., Tremonti, C., Kauffmann, G., Heckman, T., & Brinkmann, J. 2004, MNRAS, 351, 1151

Chabrier, G. 2003, ApJL, 586, L133

da Costa, L. N., Pellegrini, P. S., Davis, M., Meiksin, A., Sargent, W. L. W., & Tonry, J. L. 1991, ApJS, 75, 935

Doyle, M. T. et al. 2005, MNRAS, 361, 34

Gallego, J., Zamorano, J., Aragon-Salamanca, A., & Rego, M. 1995, ApJL, 455, L1

Garcia, A. 1993, A&AS, 100, 47

Garcia, A. M. 1995, A&A, 297, 56

Gómez, P. L. et al. 2003, ApJ, 584, 210

Grcevich, J., & Putman, M. E. 2009, ApJ, 696, 385, 0901.4975

Haynes, M. P., & Giovanelli, R. 1983, ApJ, 275, 472

Hickson, P., Kindl, E., & Auman, J. R. 1989, ApJS, 70, 687

Huang, S., Haynes, M. P., Giovanelli, R., & Brinchmann, J. 2012, ApJ, 756, 113, 1207.0523

Kennicutt, Jr., R. C. 1989, ApJ, 344, 685

——. 1998, ApJ, 498, 541

Kilborn, V. A., Forbes, D. A., Barnes, D. G., Koribalski, B. S., Brough, S., & Kern, K. 2009, MNRAS, 400, 1962, 0909.0568

Koribalski, B. S. et al. 2004, AJ, 128, 16

Lewis, I. et al. 2002, MNRAS, 334, 673

Meurer, G. R. et al. 2006, ApJS, 165, 307

Meurer, G. R. et al. 2009, ApJ, 695, 765

Meyer, M. J. et al. 2004, MNRAS, 350, 1195

Mould, J. R. et al. 2000, ApJ, 529, 786

Mulchaey, J. S. 2000, ARA&A, 38, 289

Mulchaey, J. S., & Zabludoff, A. I. 1998, ApJ, 496, 73

Nichols, M., & Bland-Hawthorn, J. 2011, ApJ, 732, 17

Pisano, D. J., Barnes, D. G., Staveley-Smith, L., Gibson, B. K., Kilborn, V. A., & Freeman, K. C. 2011, ApJS, 197, 28

Robotham, A. S. G. et al. 2012, MNRAS, 424, 1448

Rownd, B. K., & Young, J. S. 1999, AJ, 118, 670

Ryan-Weber, E. V. et al. 2004, AJ, 127, 1431

Salpeter, E. E. 1955, ApJ, 121, 161

Salzer, J. J. et al. 2000, AJ, 120, 80

Schiminovich, D. et al. 2010, MNRAS, 408, 919

Solanes, J. M., Manrique, A., García-Gómez, C., González-Casado, G., Giovanelli, R., & Haynes, M. P. 2001, ApJ, 548, 97

Stevens, J. B., Webster, R. L., Barnes, D. G., Pisano, D. J., & Drinkwater, M. J. 2004, PASA, 21, 318

Tody, D. 1993, in Astronomical Society of the Pacific Conference Series, Vol. 52, Astronomical Data Analysis Software and Systems II, ed. R. J. Hanisch, R. J. V. Brissenden, & J. Barnes, 173–+

Tully, R. B. 1987, ApJ, 321, 280

Tully, R. B. et al. 2006, AJ, 132, 729

Werk, J. K. et al. 2010, AJ, 139, 279

West, A. A., Garcia-Appadoo, D. A., Dalcanton, J. J., Disney, M. J., Rockosi, C. M., & Ivezić, Ž. 2009, AJ, 138, 796, 0910.4966

Wijesinghe, D. B. et al. 2012, MNRAS, 423, 3679

Zwaan, M. A. et al. 2004, MNRAS, 350, 1210

Table 1. Summary of Choir groups

HIPASS+ (1)	Optical ID (2)	RA [h m s] (3)	Dec [d m s] (4)	Dist. [Mpc] (5)	FOV [kpc] (6)	ELGs (7)	Comp. [kpc] (8)	M_{HI} [dex] (9)	HI Def. [dex] (10)	V_{HI} [km/s] (11)	W_{HI} [km/s] (12)	$W_{50,F}$ [km/s] (13)
J0205-55	AM 0203-552	02 05 05.48	-55 06 42.55	93	406	9	366	10.51	0.03**	6524	193	5051-8297
J0209-10	HCG 16	02 09 42.71	-10 11 01.36	54	236	4	56.2	10.31	0.18	3900	243	2560-5668
J0258-74		02 58 06.48	-74 27 22.79	70	305	4	236	10.41	-0.34	4805	399	2560-5668
J0400-52	Abell 3193	04 00 40.82	-52 44 02.72	151	659	9	420	10.61	0.13	10566	298	8182-11750
J0443-05		04 43 43.90	-05 19 09.91	69	301	5	209	10.41*	0.02	4877	278	2560-5668
J1026-19		10 26 40.81	-19 03 04.03	135	589	6	107	10.63	-0.28	9094	242	6857-9142***
J1051-17		10 51 37.46	-17 07 29.24	83	362	9	216	10.45	-0.26	5477	522	4205-7679
J1059-09	USGC S154	10 59 16.25	-09 47 38.15	122	532	10	283	10.42*	0.20	8175	80.0	6857-9142
J1159-19	ARP 022	11 59 30.13	-19 15 54.86	25	109	4	29.5	9.92	0.00	1668	150	1188-2651
J1250-20		12 50 52.84	-20 22 15.64	114	497	7	123	10.51	-0.11	7742	169	5051-8297
J1403-06	ARP 271	14 03 24.88	-06 04 09.16	41	179	4	27.5	10.29	0.09	2591	330	2217-3725
J1408-21		14 08 42.04	-21 35 49.81	128	559	6	184	10.52	0.05	8732	203	6857-9142
J1956-50		19 56 45.51	-50 03 20.30	110	480	4	299	10.52	-0.33	7446	321	4205-7679***
J2027-51	AM 2024-515	20 28 06.39	-51 41 29.83	87	380	4	224	10.44	-0.22	5881	356	4205-7679
J2318-42a	Grus Quartet	23 16 10.80	-42 35 05.00	23	100	4	73.1	10.10	0.15**	1575	222	1188-2651

Columns: (1): name assigned to field in HIPASS; (2): name assigned to group as found in NASA/IPAC Extragalactic Database (NED; http://ned.ipac.caltech.edu/); (3): J2000 right ascension of brightest source in field; (4): J2000 declination of brightest source in field; (5): distance based on the multipole attractor model as in Mould et al. (2000) and adopting H_0 = 70 km s^{-1} Mpc^{-1}; (6) field of view of ~15 arcminutes at the distance of the group; (7): number of ELGs; (8): projected group compactness, estimated by projected separation of two largest group members. See Section 3.5.; (9): logarithm of group HI mass from HIPASS. (*) We remeasured HI mass for two groups whose HIPASS measurements were incorrect. See Section 2 for more details.; (10): HI deficiency parameter defined as the logarithmic difference between the observed group HI mass and predicted group HI mass (determined by summing the predicted HI masses of the individual group galaxies). See Section 3.7 for calculation and discussion. (**) We exclude these two groups from our HI deficiency analysis due to field of view restrictions.; (11): heliocentric HI velocity; (12): observed HI emission width; (13): narrow-band filter velocity range. (***) We note that the narrow-band filters used for these two fields overlap but do not completely cover the extent of the observed HI emission width. Therefore there may be additional ELGs associated with these groups which would be classified as Choir member galaxies but are not detected in our imaging.;

Table: Catalogue of Choir members

SINGG name HiPASS+ (1)	Optical ID (2)	RA [h m s] (3)	Dec [d m s] (4)	r_e [arcsec] (5)	Axial ratio (6)	M_R [ABmag] (7)	$\log(F_{H\alpha})$ [erg/s/cm^2] (8)	μ_e [ABmag/"^{2}] (9)	Morphology (10)	Radial velocity [km/s] (11)
J0205-55:S1	ESO153-G017	02 05 05.48	-55 06 42.54	17.60±0.22	1.66	-21.95±0.22	-12.01±0.14	20.43±0.02	SAB(r)bc	6491
J0205-55:S2	ESO153-IG016	02 04 50.78	-55 13 01.55	05.19±0.00	2.26	-18.91±0.00	-12.86±0.04	21.12±0.02	SB(s)cd pec	5942
J0205-55:S3	ESO153-G015	02 04 34.92	-55 07 09.65	06.72±0.02	1.92	-21.35±0.02	-12.94±0.70	18.94±0.02	S0	
J0205-55:S4	ESO153-G013	02 04 19.75	-55 13 50.44	11.25±0.09	3.45	-21.39±0.09	-12.61±0.34	20.02±0.02	Sa:	5942
J0205-55:S5	APMUKS	02 04 54.77	-55 08 31.99	05.84±0.18	2.19	-17.13±0.18	-14.45±0.36	23.28±0.02	[D]	6127
J0205-55:S6	APMUKS	02 04 57.07	-55 13 34.10	02.52±0.06	1.56	-18.14±0.06	-14.13±0.36	20.38±0.03	[D]	5760
J0205-55:S7	6dF	02 05 00.57	-55 15 19.63	01.87±1.08	1.54	-15.65±1.08	-14.35±0.29	22.35±0.35	cD	5760
J0205-55:S8	APMUKS	02 04 29.71	-55 12 56.09	02.61±0.05	1.03	-17.44±0.05	-14.69±0.69	21.21±0.02	cD	
J0205-55:S9*	APMUKS	02 05 23.76	-55 14 14.20	01.06±0.21	–	-15.37±0.12	-14.39±0.46	18.78±0.45	cD	
J0209-10:S1	NGC0839	02 09 42.71	-10 11 01.36	11.93±0.12	2.32	-21.00±0.12	-12.11±0.11	19.44±0.02	Spec sp; LINER Sy2	
J0209-10:S2	NGC0838	02 09 38.48	-10 08 45.79	07.97±0.07	1.33	-21.16±0.07	-11.38±0.03	18.36±0.02	SA(rs)0° pec: Sbrst	
J0209-10:S3	NGC0835	02 09 24.43	-10 08 10.59	16.04±0.18	2.25	-21.47±0.18	-11.90±0.12	19.53±0.03	SAB(r)ab: pec LINER	
J0209-10:S4	NGC0833	02 09 20.69	-10 07 58.55	08.87±0.01	1.73	-21.14±0.01	-12.68±0.49	18.63±0.02	(R')SA:pec;Sy2 LINER	
J0258-74:S1	ESO031-G005	02 58 06.48	-74 27 22.79	20.25±0.26	2.81	-21.50±0.26	-12.06±0.09	20.47±0.02	SAB(rs)bc HII	
J0258-74:S2	MRSS	02 58 52.43	-74 25 53.25	10.34±0.29	1.22	-19.15±0.29	-13.04±0.08	21.66±0.03	[S]	
J0258-74:S3	2MASX	02 58 42.76	-74 26 03.55	06.72±0.56	3.40	-18.25±0.56	-13.47±0.12	21.70±0.09	[S]	
J0258-74:S4	MRSS	02 57 29.23	-74 22 34.75	04.07±0.85	1.31	-17.13±0.85	-14.05±0.33	21.80±0.27	[dIrr]	
J0400-52:S1	ESO156-G029	04 00 40.82	-52 44 02.71	06.80±0.06	1.22	-21.32±0.06	-12.84±0.20	20.11±0.02	SA(rs)cd pec:	
J0400-52:S2	APMUKS	04 00 48.07	-52 41 02.81	01.75±0.02	1.44	-15.78±0.02	-14.67±0.10	23.15±0.02	[S]	
J0400-52:S3	2MASX	04 00 06.03	-52 39 32.63	02.95±0.01	1.64	-19.64±0.01	-13.61±0.20	20.18±0.02	[S]	
J0400-52:S4	IC2028	04 01 18.23	-52 42 27.08	08.10±0.01	1.47	-22.07±0.01	-12.63±0.31	19.57±0.02	Scd:	
J0400-52:S5	2MASX	04 00 53.00	-52 49 38.43	09.41±0.05	1.42	-21.98±0.05	-12.65±0.30	20.01±0.02	(R)SB(s)b? pec	
J0400-52:S6	IC2029	04 01 17.84	-52 48 02.81	12.08±0.06	1.80	-21.50±0.06	-13.05±0.42	21.13±0.02	SB(s)c pec	
J0400-52:S7	APMUKS	04 01 08.99	-52 49 32.78	03.72±0.13	1.59	-18.61±0.13	-14.08±0.23	21.81±0.04	[D]	
J0400-52:S8*	-	04 01 17.00	-52 42 08.50	02.07±0.35	–	-17.36±0.08	-14.20±0.52	16.46±0.37	[D]	
J0400-52:S9*	-	04 01 19.29	-52 47 56.10	03.46±1.38	–	-17.56±0.07	-14.09±0.57	15.15±0.87	[D]	
J0443-05:S1	NGC1643	04 43 43.90	-05 19 09.93	10.71±0.21	1.19	-21.52±0.21	-11.65±0.04	19.05±0.04	SB(r)bc pec?	
J0443-05:S2	NGC1645	04 44 06.43	-05 27 56.31	16.90±0.15	1.99	-21.87±0.15	-12.15±0.20	19.62±0.02	(R')SB(rs)0+ pec	
J0443-05:S3	2MASX	04 44 11.67	-05 14 38.31	04.79±0.19	1.86	-19.56±0.19	-13.38±0.25	19.53±0.06	[S]	
J0443-05:S4	2MASX	04 44 05.54	-05 25 46.50	04.95±0.12	1.60	-18.77±0.12	-13.07±0.06	20.46±0.03	[D]	

Table 2: Choir member descriptions.

Columns: (1): Name assigned in SINGG (HiPASS name with :Sn appended for nth source; (2) Previously assigned ID based on position match with NASA/IPAC Extragalactic Database (NED; http://ned.ipac.caltech.edu/); (3): Right Ascension (J2000); (4): Declination (J2000); (5): R-band effective radius; (6): Ratio of major and minor axes; (7): R-band absolute magnitude; (8): Logarithm of total Hα flux, corrected for Galactic extinction and [NII] contamination; (9): R-band effective surface brightness, face-on and extinction-corrected (Galactic and internal); (10): NED morphological classification where available, or [new classification]; (11): Central radial velocity from our ANU2.3mT/WiFeS data (Sweet. et al., in prep). Sources marked with * have been identified since SINGG release 1; for these we give preliminary measurements performed using IRAF's APPHOT task. IRAF is distributed by the National Optical Astronomy Observatories, which are operated by the Association of Universities for Research in Astronomy, Inc., under cooperative agreement with the National Science Foundation (Tody, 1993). ** Our declination for J1250-20:S3 is 10" different to the ESO measurement, suggesting a problem with their search radius for this object. *** Only half of J2318-42a is within our FOV, so we use the NED position for J2318-42a:S3.

Table: continued from previous page

SINGG name HIPASS+ (1)	Optical ID (2)	RA [h m s] (3)	Dec [d m s] (4)	r_e [arcsec] (5)	Axial ratio (6)	M_R [ABmag] (7)	$\log(F_{H\alpha})$ [erg/s/cm^2] (8)	μ_e [ABmag/"^{2}] (9)	Morphology (10)	Radial velocity [km/s] (11)
J0443-05:S5*	SEGC	04 43 45.02	-05 19 41.90	01.97±0.98	—	-17.65±0.04	-13.47±0.91	14.62±1.09	S0+? pec	
J1026-19:S1	ESO568-G011	10 26 40.81	-19 03 04.01	11.86±0.19	1.28	-22.01±0.19	-12.49±0.35	20.12±0.03	SAB(s)bc: pec Sbrst	
J1026-19:S2	2MASX	10 26 50.07	-19 04 31.77	05.46±0.20	1.36	-20.16±0.20	-13.04±0.15	20.57±0.05	Irr	
J1026-19:S3	-	10 26 18.93	-18 57 52.12	04.68±0.27	1.45	-18.41±0.27	-14.36±0.54	22.16±0.03	[D]	
J1026-19:S4	-	10 26 24.40	-19 02 02.99	02.19±0.26	1.38	-17.62±0.26	-14.26±0.35	21.35±0.11	[dIrr]	
J1026-19:S5	-	10 26 42.07	-19 07 35.07	05.56±0.60	1.55	-16.87±0.60	-14.67±0.42	24.17±0.04	[dIrr]	
J1026-19:S6	FLASH	10 26 25.21	-19 10 35.31	07.91±0.07	1.10	-19.83±0.07	-14.27±1.67	21.75±0.02	S0	
J1051-17:S1	2MASX	10 51 37.45	-17 07 29.23	27.62±0.26	1.76	-21.01±0.26	-12.62±0.26	22.12±0.02	(R?+PR?)	5485
J1051-17:S2	NGC3431	10 51 15.11	-17 00 29.44	14.72±0.05	2.47	-21.25±0.05	-12.40±0.21	20.46±0.02	SABb?	5302
J1051-17:S3	-	10 51 35.94	-16 59 16.80	06.61±0.05	1.02	-17.91±0.05	-13.72±0.13	22.43±0.02	[dS]	5988
J1051-17:S4	-	10 51 26.01	-17 05 03.61	03.48±0.09	1.40	-16.19±0.09	-14.51±0.19	22.84±0.02	[dIrr]	5485
J1051-17:S5	-	10 51 50.91	-16 58 31.64	03.58±0.06	1.75	-17.02±0.06	-14.35±0.33	22.03±0.02	[dIrr]	5485
J1051-17:S6	-	10 51 42.78	-17 06 34.59	02.11±0.04	1.29	-16.78±0.04	-14.18±0.13	21.14±0.02	[cD]	5668
J1051-17:S7	-	10 51 33.36	-17 08 36.63	04.18±0.12	1.53	-16.77±0.12	-14.28±0.21	22.63±0.02	[cD]	5394
J1051-17:S8*	-	10 51 25.92	-17 08 16.44	01.52±0.67	—	-17.48±0.04	-13.46±0.88	15.44±0.97	[dS]	5314
J1051-17:S9*	-	10 51 56.54	-17 05 03.50	00.34±0.17	—	-16.68±0.05	-13.78±0.71	19.51±1.09	[dE,N]	5606
J1059-09:S1	MCG-01-28-013	10 59 16.25	-09 47 38.16	15.08±0.20	1.91	-22.26±0.20	-12.12±0.12	20.20±0.03	SAB(rs)b pec:	
J1059-09:S2	GNX034	10 59 06.77	-09 45 04.38	11.72±0.24	1.36	-19.80±0.24	-12.91±0.05	22.51±0.02	[Irr]	
J1059-09:S3	MCG-01-28-012	10 59 15.61	-09 48 59.41	14.66±0.37	3.13	-20.84±0.37	-12.51±0.06	21.82±0.03	Sab pec sp	
J1059-09:S4	MRK1273	10 58 46.84	-09 50 43.31	08.79±0.15	1.32	-21.53±0.15	-12.48±0.12	19.91±0.03	SB0-a Sbrst	
J1059-09:S5	GNX066	10 59 30.98	-09 44 25.26	09.11±0.13	2.84	-19.57±0.13	-13.15±0.08	22.21±0.02	[S]	
J1059-09:S6	-	10 59 08.46	-09 43 14.49	08.04±0.16	1.69	-19.00±0.16	-13.54±0.12	22.56±0.02	[Irr]	
J1059-09:S7	-	10 59 21.31	-09 47 50.49	02.50±0.15	1.59	-18.83±0.15	-13.47±0.08	20.21±0.06	[cD]	
J1059-09:S8	-	10 59 01.73	-09 52 46.76	03.46±0.40	1.81	-16.81±0.40	-14.91±0.41	23.07±0.10	[D]	
J1059-09:S9*	-	10 58 44.69	-09 53 28.60	00.59±0.29	—	-13.56±0.10	-14.38±0.43	19.58±1.09	[dIrr]	
J1059-09:S10*	2MASX	10 59 02.64	-09 53 19.90	00.37±0.07	—	-17.03±0.02	-16.16±0.44	17.13±0.44	[dS]	
J1159-19:S1	NGC4027	11 59 30.13	-19 15 54.88	34.37±0.13	1.07	-21.24±0.13	-10.97±0.04	19.71±0.02	SB(s)dm HII	
J1159-19:S2	NGC4027A	11 59 29.34	-19 19 59.52	16.26±0.10	1.40	-17.83±0.10	-12.83±0.06	21.86±0.02	IB(s)m:	
J1159-19:S3	-	11 59 35.79	-19 19 02.99	03.80±0.29	1.00	-15.18±0.29	-14.21±0.28	21.48±0.06	[D]	
J1159-19:S4	ISZ108A	11 59 37.88	-19 19 45.80	06.18±0.36	1.34	-15.77±0.36	-14.04±0.23	21.91±0.05	[D]	

Table 2: Choir member descriptions.

Columns: (1): Name assigned in SINGG (HIPASS name with :Sn appended for nth source; (2) Previously assigned ID based on position match with NASA/IPAC Extragalactic Database (NED; http://ned.ipac.caltech.edu/); (3): Right Ascension (J2000); (4): Declination (J2000); (5): R-band effective radius; (6): Ratio of major and minor axes; (7): R-band absolute magnitude; (8): Logarithm of total Hα flux, corrected for Galactic extinction and [NII] contamination; (9): R-band effective surface brightness, face-on and extinction-corrected (Galactic and internal); (10): NED morphological classification where available, or [new classification]; (11): Central radial velocity from our ANU2.3mT/WiFeS data (Sweet, et al., in prep). Sources marked with * have been identified since SINGG release 1; for these we give preliminary measurements performed using IRAF's APPHOT/Mask. IRAF is distributed by the National Optical Astronomy Observatories, which are operated by the Association of Universities for Research in Astronomy, Inc., under cooperative agreement with the National Science Foundation (Tody, 1993). ** Our declination for J1250-20:S3 is 10" different to the ESO measurement, suggesting a problem with their search radius for this object. *** Only half of J2318-42a is within our FOV, so we use the NED position for J2318-42a:S3.

Table: continued from previous page

SINGG name HIPASS+ (1)	Optical ID (2)	RA [h m s] (3)	Dec [d m s] (4)	r_e [arcsec] (5)	Axial ratio (6)	M_R [ABmag] (7)	$\log(F_{H\alpha})$ [erg/s/cm^2] (8)	μ_e [ABmag/$''^2$] (9)	Morphology (10)	Radial velocity [km/s] (11)
J1250-20:S1	ESO575-G006	12 50 52.84	-20 22 15.65	09.95±0.13	1.38	-21.85±0.13	-12.17±0.10	19.58±0.03	SA(s)bc pec HII	
J1250-20:S2	ESO575-G004	12 50 40.91	-20 20 06.22	10.09±0.04	1.37	-21.44±0.04	-12.44±0.11	20.09±0.02	S	
J1250-20:S3**	eso-lv5750061	12 50 49.77	-20 22 03.44	04.25±0.14	1.54	-18.57±0.14	-13.36±0.07	21.43±0.04	[Irr]	
J1250-20:S4	-	12 50 39.92	-20 20 52.87	05.93±0.11	1.59	-18.72±0.11	-13.95±0.20	21.98±0.03	[Irrs]	
J1250-20:S5	-	12 50 59.16	-20 28 14.80	02.66±0.27	2.04	-17.43±0.27	-13.84±0.15	21.64±0.10	[cD]	
J1250-20:S6*	-	12 50 45.87	-20 23 30.10	0.154±0.51	–	-15.38±0.15	-14.39±0.43	18.42±0.74	[D]	
J1250-20:S7*	-	12 50 46.92	-20 23 12.40	01.28±0.51	–	-14.16±0.27	-14.83±0.25	20.04±0.91	[D]	
J1403-06:S1	NGC5426	14 03 24.88	-06 04 09.14	29.64±0.35	1.99	-21.18±0.35	-11.38±0.03	20.57±0.02	SA(s)c pec	2512
J1403-06:S2	NGC5427	14 03 26.09	-06 01 51.20	36.45±0.09	1.30	-22.01±0.09	-11.11±0.04	20.05±0.02	SA(s)c pec;Sy2 HII	2741
J1403-06:S3	APMUKS	14 03 13.48	-06 06 24.17	04.18±0.85	1.03	-15.27±0.85	-14.40±0.26	22.70±0.17	[cD]	2767
J1403-06:S4	APMUKS	14 03 34.62	-06 07 59.27	05.96±0.86	1.43	-14.42±0.86	-14.85±0.34	24.34±0.02	[cD]	2685
J1408-21:S1	ESO578-G026	14 08 42.04	-21 35 49.82	10.24±0.26	1.47	-22.35±0.26	-12.24±0.07	19.22±0.05	SB(r1)c	8704
J1408-21:S2	2MASX	14 08 57.72	-21 38 52.47	07.99±0.06	1.39	-21.11±0.06	-12.67±0.04	20.15±0.02	[S]	8831
J1408-21:S3	2MASX	14 08 41.04	-21 37 40.97	06.06±0.10	1.60	-20.26±0.10	-13.19±0.07	20.52±0.03	[S0]	8792
J1408-21:S4	2MASX	14 08 33.28	-21 36 07.18	09.21±0.08	1.18	-20.72±0.08	-13.35±0.12	20.92±0.02	[S0]	9137
J1408-21:S5*	-	14 08 39.82	-21 38 14.30	00.58±0.58	–	-13.31±0.52	-15.16±0.06	22.89±2.24	[cD]	8788
J1408-21:S6*	-	14 08 52.84	-21 42 07.20	01.73±0.58	–	-17.12±0.07	-14.30±0.48	16.70±0.73	[dS]	8682
J1956-50:S1	IC4909	19 56 45.51	-50 03 20.29	15.70±0.19	2.42	-21.68±0.19	-12.38±0.16	20.70±0.03	SA:(rs:)bc	7634
J1956-50:S2	2MASX	19 55 53.21	-50 02 10.82	08.03±0.11	1.29	-20.32±0.11	-12.69±0.08	20.81±0.02	[S/Irr]	7039
J1956-50:S3	-	19 56 08.20	-50 02 21.56	01.72±0.22	1.01	-16.49±0.22	-13.67±0.05	21.59±0.11	[BCD]	6400
J1956-50:S4*	-	19 55 45.92	-50 06 15.50	01.74±0.74	–	-15.15±0.23	-14.60±0.10	19.23±0.96	[cD]	7497
J2027-51:S1	ESO234-G032	20 28 06.39	-51 41 29.83	12.49±0.29	1.89	-21.15±0.29	-12.03±0.06	20.34±0.03	(R')SB(s)bc	5805
J2027-51:S2	ESO234-G028	20 27 31.97	-51 39 20.81	16.13±0.17	1.66	-21.31±0.17	-12.13±0.08	20.71±0.02	SAB(s)bc pec	5805
J2027-51:S3	MRSS	20 27 48.52	-51 44 19.35	05.57±0.12	1.59	-18.93±0.12	-13.20±0.11	21.07±0.03	[dIrr]	5805
J2027-51:S4	-	20 27 54.64	-51 38 04.52	02.05±0.15	1.15	-17.20±0.15	-13.71±0.14	20.74±0.04	[cD]	5988
J2318-42a:S1	NGC7582	23 18 23.44	-42 22 11.94	51.63±0.26	1.98	-21.60±0.26	-11.02±0.07	20.04±0.02	(R')SB(s)ab Sy2	1436
J2318-42a:S2	NGC7590	23 18 54.78	-42 14 18.94	26.70±0.05	2.15	-20.71±0.05	-11.12±0.03	19.64±0.02	S(r?)bc Sy2	1457
J2318-42a:S3***	NGC7599	23 19 21.14	-42 15 24.6	38.99±0.29	2.03	-19.76±0.29	-11.87±0.06	21.53±0.02	SB(s)c	1753
J2318-42a:S4*	APMUKS	23 18 50.44	-42 23 50.30	00.49±0.41	–	-11.45±0.17	-14.77±0.27	20.72±1.82	[LSBD]	1661

APPENDIX A: NOTES ON INDIVIDUAL CHOIR GROUPS

By "member" we refer to objects with apparent Hα emission in the filter used for the SINGG images. We note that these are likely groups; spectroscopic redshifts are needed to confirm membership, especially for the small, faint galaxies. We also searched larger 40-arcminute photographic survey images[3] centred on the brightest member of each group (named "S1") to check for any bright galaxies that could be group members.

HIPASS J0205-55: The field HιPASS J0205-55 covers two sources: HιPASS J0205−55a at V_{hel} = 6524 km s^{-1} and HιPASS J0205−55b at V_{hel} = 5964 km s^{-1} (Meyer et al. 2004). We note that HιPASS J0205−55a is included in the SINGG sample selection while HιPASS J0205−55b is not (Meurer et al. 2006), Our observations show a total of 9 galaxies in this rich field: 4 giant spirals and 5 dwarfs of varying sizes. The smallest (S8, S9) are almost in the ELdot category. The galaxies S1, S2, S3, S4, and S6 have published velocities of 6528, 5927, 6131, 5864, and 5756 km s^{-1} respectively (da Costa et al. 1991). Hence S1 is associated with HιPASS J0205−55a; S2, S4 and S6 are associated with HιPASS J0205−55b; while S3 is at an intermediate velocity. The existence of galaxies at velocities between the a and b components suggest that the two component systems are merging. The extended optical image of this group reveals one additional large galaxy, ESO153-G020 (velocity 5197 km s^{-1}) associated with HιPASS J0205−55b (Doyle et al. 2005).

HIPASS J0209−10: The galaxies of this group show strong signs of interactions, all being classified "pec" and most having extensive extraplanar gas in the Hα images. The group appears in several group catalogues, most notably it is Hickson Compact Group 16. We found no new Hα-emitting galaxies compared to Meurer et al. (2006) which has a more detailed description of the members in its Appendix B. (There is a fainter galaxy 1.5' to the NE of S3 = NGC0835, SDSS J020928.18-100653.6 but it is a background object, velocity = 25706 km s^{-1}.) The extended optical image of this group reveals one additional large galaxy, NGC 0848 (velocity 3989 km s^{-1}) also likely to be associated with the group (Garcia 1993).

HIPASS J0258−74: A typical small group with three spirals and one tiny dwarf irregular galaxy.

HIPASS J0400−52: Part of an extensive cluster (Abell 3193) with a total of 9 members identified: 4 spirals and 5 dwarfs of varying sizes; two of these are very small companions to the giant S4 and S6 galaxies. The extended optical image of this group reveals two additional large galaxies, NGC 1506 (10271 km s^{-1}) and ESO156-G031 (10467 km s^{-1}) at 10 and 15 arcminutes from the central galaxy S1 respectively. These are both classified as S0 galaxies, so although associated with the group they are unlikely to contain large amounts of HI.

HIPASS J0443−05: An extended group of three large spirals, two with companions. The line emission of S5, an apparent companion to S1, is weak and needs to be confirmed.

HIPASS J1026−19: This group is dominated by a single face-on giant spiral (S1) which is connected to S2 by a tidal tail. The 4 other members are small and well-separated, notably S3 which is on the very edge of the image.

HIPASS J1051−17: This extensive group has 9 members distributed over much of the image. The galaxy S9 is notable for being an apparent dE,N galaxy with weak nuclear Hα emission. The extended images reveals one additional large Sa galaxy, MCG-03-28-016 (6220 km s^{-1}, 9 arcminutes from S1) which may possibly be associated with the group (5491 km s^{-1}).

HIPASS J1059−09: This group features a strongly-interacting galaxy pair (S1 and S3) as well as several other spirals. The two newly-measured galaxies are S9, a small, lopsided dwarf with one HII region, and S10, an edge-on disk galaxy with faint apparent residual Hα in the central region as well as weak, very low surface brightness Hα along the NW minor axis. S10 is a confirmed group member (2MASX J10590262−0953197 at velocity 8229 km s^{-1}) and there are signs of interaction between it and S8, a possible low-surface brightness group member. The extended image reveals a bright galaxy, MCG-01-28-020, at 15 arcminutes from S1 but its velocity (11779 km s^{-1}) makes it a background object.

HIPASS J1159−19: This compact group of 4 galaxies features a nearly face-on late-type spiral with bright Hα emission, and 3 dwarfs to the S and SE. The field is also known as Arp 022 and is near to the well-known Antennae group, Arp 244.

HIPASS J1250−20: This is a typical group with two large spirals and 3 dwarf companions, but we also note the detection of two very compact Hα emitters (S6 and S7) that may be on a tidal tail extending from S1. These are strong candidates for tidal dwarf galaxies in formation.

HIPASS J1403−06: This small group (4 members) is dominated by two strongly-interacting spirals catalogued as Arp 271, and also contains two faint ELdot-like dwarfs.

HIPASS J1408−21: The central galaxy of this group, S1 shows extended emission. The arm pointing South to S3 shows possible tidal distortion in the Hα emission. There are two new galaxies in the field: S5 and S6. S5 is barely resolved with a single faint HII region and located to the SW of S3, possibly at the extreme end of the tidal arm extending from S1. S6 appears to have weak residual Hα in the nuclear region of a small, high-inclination disk, but may be due to bad continuum subtraction in a background galaxy. The extended image reveals a bright galaxy, ESO 578-G030, 11 arcmin from S1 but its velocity (10891 km s^{-1}) makes it a background object.

HIPASS J1956−50: This group consists of a large spiral, S1 to the East, a late type spiral or irregular, S2, to the West, a nearly ELdot-like blue compact dwarf, S3, projected between them and a new, faint compact dwarf S4 near the W edge of the frame which is difficult to spot due to nearby bad

---

[3] Digitised Sky Survey images in the blue (B_J) band from the Canadian Astronomy Data Centre.
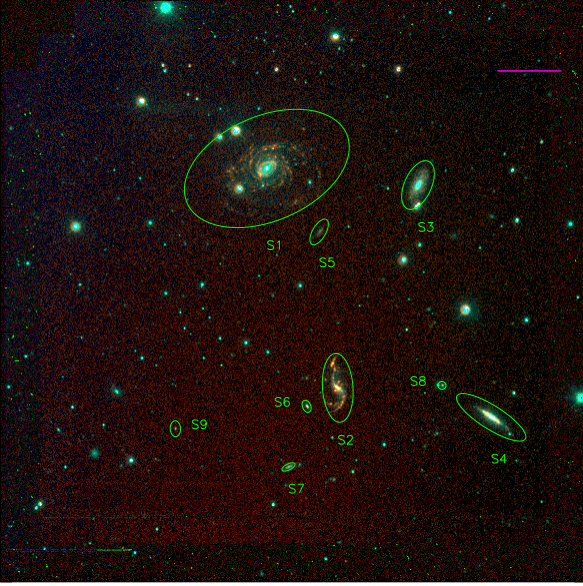
Figure B1. Choir group at HɪPASS J0205-55. Colours are assigned as follows: R is displayed in the blue channel, the narrowband Hα in the green channel, and the net Hα shown in the red channel. ELGs thus appear red. Aperture colours are as follows: green denotes ELGs measured in SINGG, while yellow indicates newly-discovered ELGs. Each image is 15.5 arcminutes on a side. The magenta scale bars indicate 50kpc. North is up and East is left. (Figures B1 to B15 make use of this colour scheme, scale and orientation.)

columns in the data. The large velocity spread of these objects (see Table B1) indicates that group membership needs to be confirmed for this group.

HIPASS J2027−51: This group contains two large distorted spirals, S1 and S2, a dwarf irregular, S3, and compact near ELdot dwarf, S4. The data are relatively noisy, so may contain faint undetected members in addition to the 4 listed.

HIPASS J2318−42a: This nearby (1603 km s^{-1}) group consists of four large spiral galaxies: NGC 7582, NGC 7590, NGC 7599, plus NGC 7552 which is not visible in the fields of our optical images. The group is known as the "Grus Quartet" (see Koribalski et al. 2004). We have identified one very faint additional group member in our Hα imaging, denoted S4 in our table: this is one of the faintest group dwarf galaxies in our sample, but follow-up observations have confirmed that it is a group member (Sweet et al., in prep.).

APPENDIX B: IMAGES

Figure B2. HɪPASS J0209-10

Figure B3. HɪPASS J0258-74

Figure B4. HιPASS J0400-52

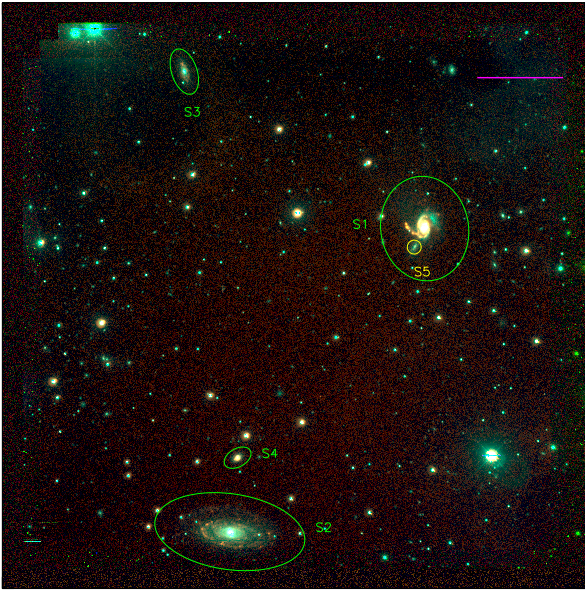**Figure B6.** HιPASS J1026-19

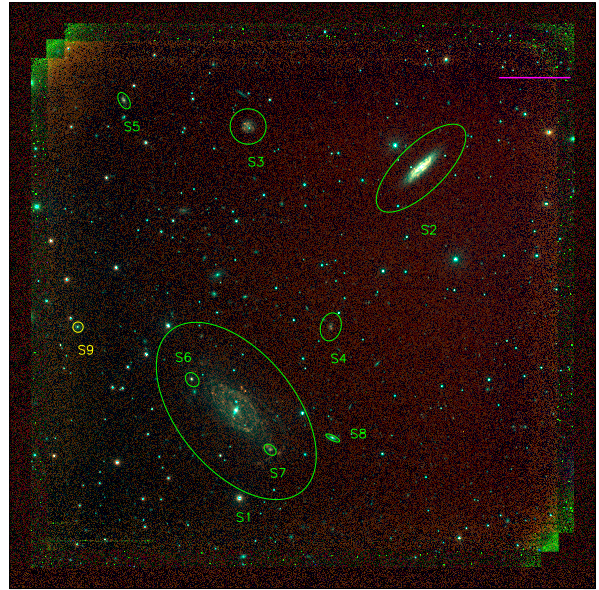**Figure B5.** HιPASS J0443-05

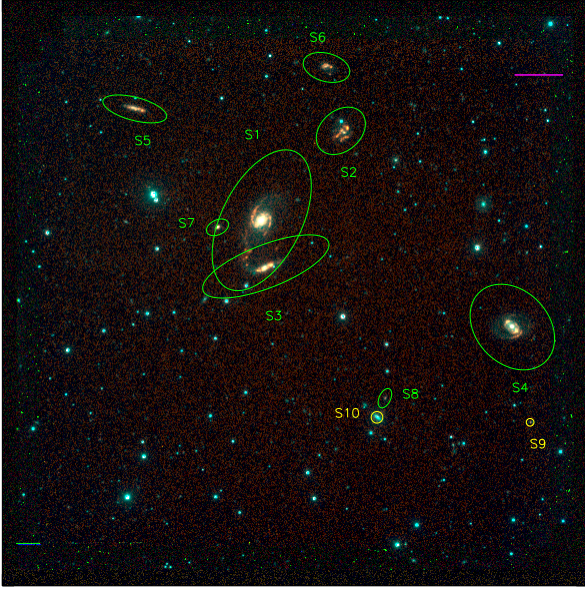**Figure B7.** HιPASS J1051-17

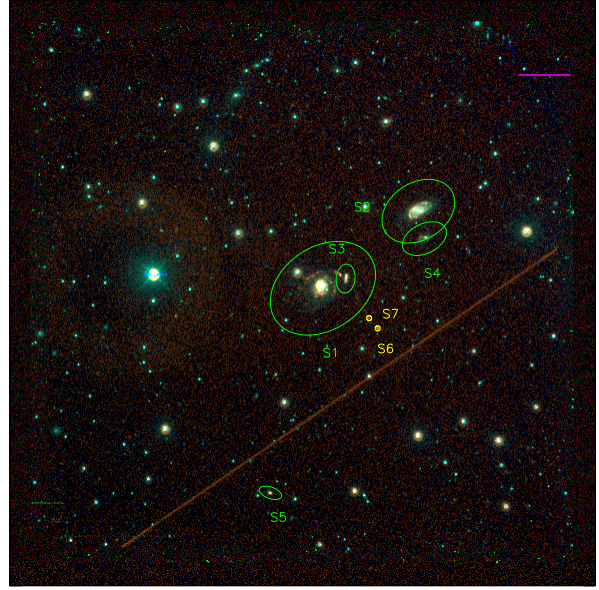**Figure B8.** HIPASS J1059-09

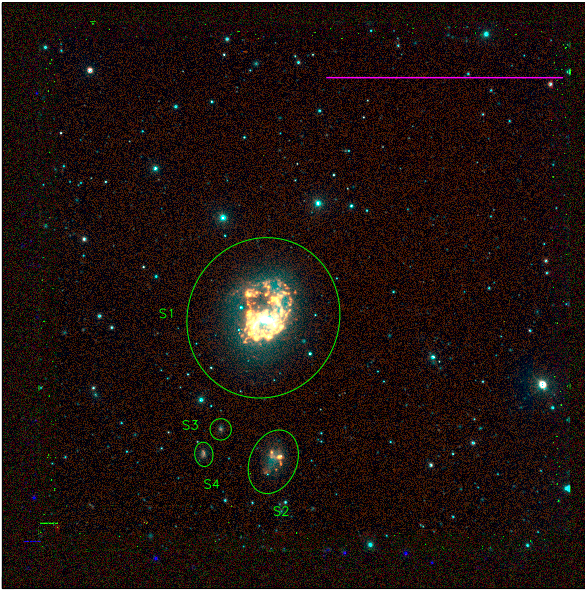

Figure B10. HIPASS J1250-20
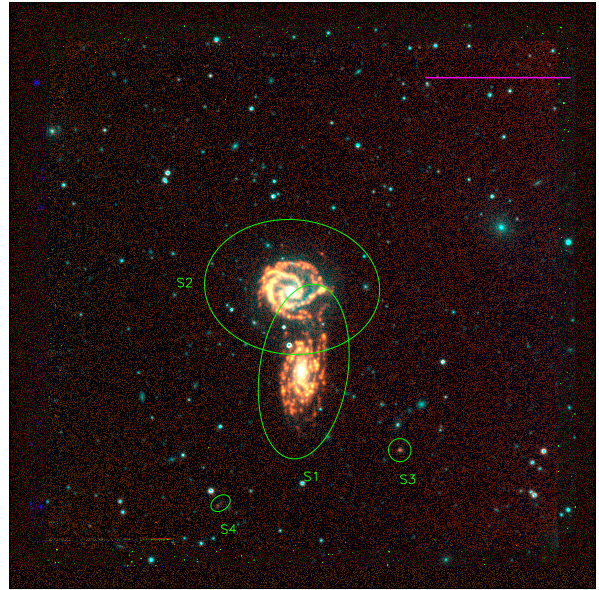

Figure B9. HIPASS J1159-19
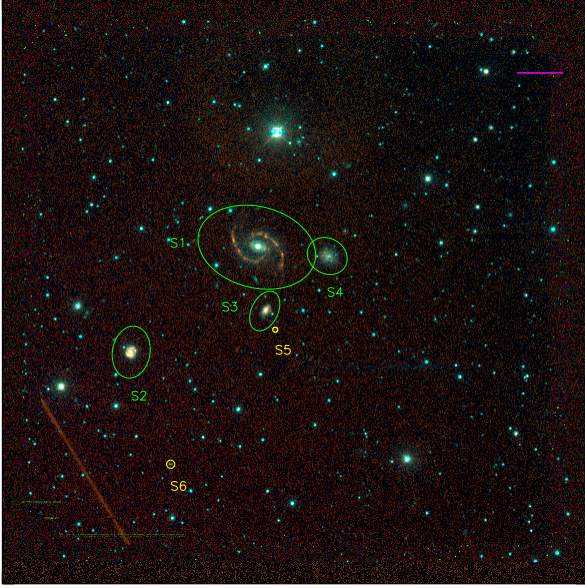

Figure B11. HIPASS J1403-06

Figure B12. HIPASS J1408-21
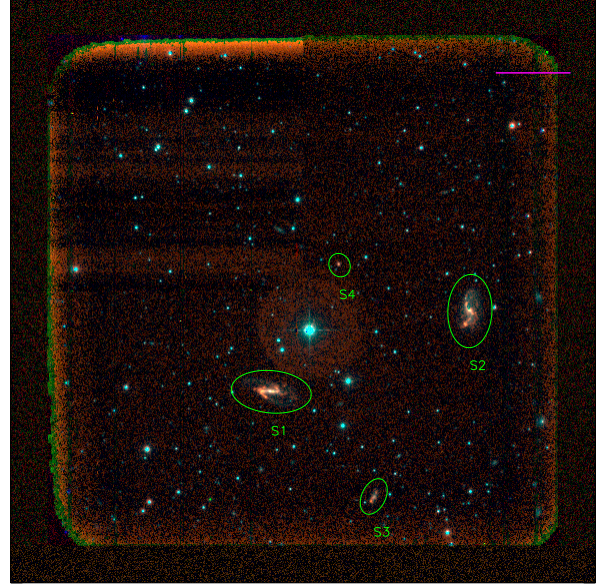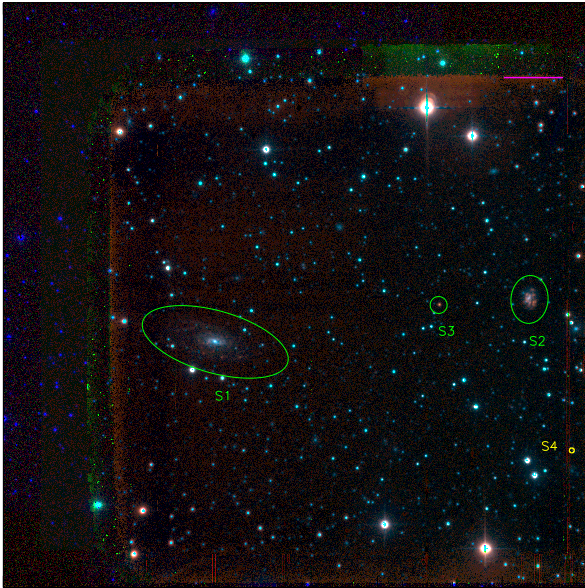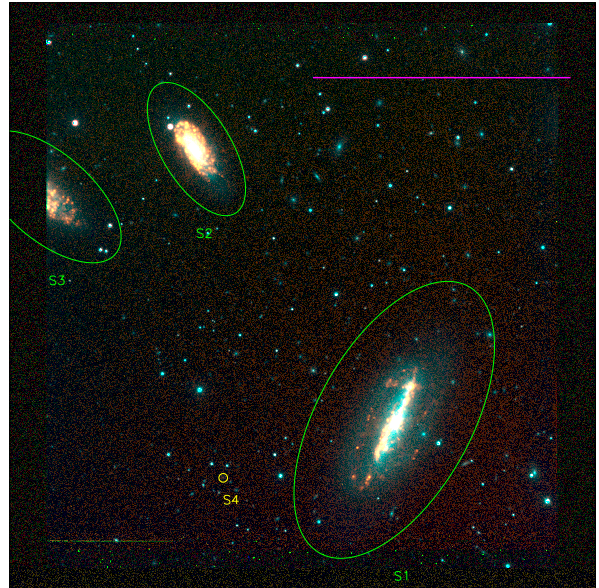

Figure B14. HIPASS J2027-51

Figure B13. HIPASS J1956-50

Figure B15. HIPASS J2318-42a